

POLITECNICO DI TORINO

Master's Degree in Mathematical Engineering



**Politecnico
di Torino**



Stochastic processes for collective dynamics of self-propelled particles

Supervisors

Prof. Luigi PREZIOSI

Dr. Gianni PAGNINI

Prof. Scott HOTTOVY

Candidate

Andrea FIORESE

March 2023

Summary

In the last years, collective motions have fascinated and attracted the attention of the scientific community. Indeed, this type of phenomena is ubiquitous in nature and often it is of rare beauty, just think about the dance of a large swarm of starlings during last hours of the day. It is also impressive how ordered patterns and coherent behaviour emerge from the interactions among individuals. In this Thesis, we propose a new microscopic model based on a system of interacting stochastic differential equations of Langevin-type for describing the collective dynamics of a self-propelled particle swarm. The concept of self-propelled particles is of crucial importance in modeling the behaviour of animal groups or of cell populations. Indeed, agents of biological systems are capable of persistent and active motion, and they can freely move by virtue of their internal metabolism. There is a rich literature about swarming behaviour, and we formulated our model by carefully choosing mathematical tools and assumptions. In many of available models the swarm dynamics is settled in the overdamped regime. Here we formulate a stochastic dynamical process by adopting an underdamped approach. In our model we combined three well known forces. First a Morse-type potential that accounts for social interactions within the swarm. A friction force that has the role of a restoration term for the microscopic dynamics. Finally, an alignment term that stimulates particles to assume the velocity of their neighbours via a weighted average procedure. This alignment term has been proven to have a central role in leading the swarm dynamics, as it has been shown in several papers in literature (see, for example, [1], or [13]). In particular, we first derive the equation of motion for the center of mass, and later we identify three different dynamical regimes for the swarm dynamics that correspond to the balancing between the alignment and friction effects. Moreover, numerical simulations have been performed for supporting the theoretical results. To conclude, we studied the role and the effect of the finiteness of the swarm ensemble. We found that such finiteness is responsible for the emerging of random fluctuations in the motion of the center of mass of the swarm, which is ruled by a stochastic motion as well: the statistical characterisation of this stochastic motion has been derived.

Acknowledgements

Credo che questa sia una parte personale del mio lavoro di tesi, e perciò credo di potermi esprimere nella mia lingua madre, con cui mi sento maggiormente a mio agio per tutto ciò che non concerne l'ambito scientifico.

Per cominciare, voglio ringraziare di cuore la mia famiglia, i miei genitori e mio fratello, che mi hanno sempre sostenuto in questi anni. Vi sono diverse accezioni che qui assume la parola "sostenere". Può ammantarsi, per esempio, del significato di sostentamento economico, peraltro essenziale, ma quello che più mi preme sottolineare è la loro costante presenza, il loro appoggio in ogni situazione. Fosse esso per consolarmi di un insuccesso e incoraggiarmi, o per farmi voltare lo sguardo verso un punto più luminoso e ricordarmi che le cose sono ciò che sono solo perché le osserviamo da una certa prospettiva.

Voglio poi ringraziare il professor Luigi Preziosi, sia per aver accettato di ricoprire il ruolo di relatore in questo mio lavoro di tesi, sia per le sue magnifiche lezioni che ho seguito con passione durante la magistrale al Politecnico di Torino. Accendere una scintilla di interesse è senza dubbio un passo fondamentale.

Ringrazio anche il professor Scott Hottovy, per la sua pazienza e disponibilità, ma soprattutto per le interessantissime discussioni alla lavagna, durante le quali hanno preso forma alcuni dei risultati matematici che sono al cuore di questo mio lavoro ¹. Voglio ringraziare poi Gianni Pagnini, mio tutor presso il BCAM. Sono profondamente felice di aver fatto la sua conoscenza e di aver condiviso parte di questi mesi. Oltre al suo contributo essenziale nello sviluppare il presente elaborato, mi ha dato ottimi consigli su Bilbao aiutandomi ad ambientarmi in una città a me completamente nuova. Forse però, il suo contributo che più ho apprezzato, è stato mostrarmi che una ricerca scientifica di buona qualità si basa soprattutto su un autentico interesse, e che, anche se è importante riconoscere l'esperienza del proprio mentore, la distanza che spesso separa studente e professore può essere assottigliata, così da giungere ad un rapporto più limpido e produttivo (vorrei dire

¹"I want also to thank professor Scott Hottovy, for his patience and availability, but above all for the really interesting discussions on the blackboard, during which some of the mathematical results that are at the heart of this work have taken shape."

che tende all'amicizia, ma potrebbe scalfire la patina di formalità consona a tale occasione).

Voglio poi ringraziare tutti i miei amici, di Trento, Torino e Bilbao, che mi hanno accompagnato lungo il cammino e hanno colorato il mio tempo. Per quanto sia vivace e gorgogliante di mille opportunità, credo che ciò che veramente ci fa sentire a casa in un luogo siano le persone a cui ci leghiamo.

Voglio infine ringraziare il BCAM (Basque Center for Applied Mathematics) per avermi dato la possibilità di soggiornare a Bilbao e di svolgere l'attività di ricerca che in questi ultimi mesi ha portato al mio lavoro di tesi. Ritengo sia stata un'esperienza alquanto stimolante e chiarificatrice per il mio futuro.

Table of Contents

List of Figures	VIII
1 Introduction on Swarm Models	1
1.1 Swarming behaviour in biology	1
1.2 Different modelling approaches	3
1.3 Brief overview on existing particle models	6
1.3.1 Vicsek model	6
1.3.2 D’Orsogna-Bertozzi model	7
1.3.3 Cucker-Smale model	8
1.3.4 Swarming models with leaders	10
2 Mathematical Model	12
2.1 Introduction to the current model	12
2.2 Swarm center of mass equations	15
2.3 Statistical analysis of the center of mass equations	18
2.3.1 Swarm center of mass velocity equation	18
2.3.2 Swarm center of mass position equation	20
3 Numerical simulations	28
3.1 Methods	29
3.2 Comparison between microscopic dynamics and deterministic results	31
3.2.1 The accelerated regime	31
3.2.2 The wandering center of mass regime	36
3.2.3 The invariant regime	40
3.3 Numerical simulations of statistical results	43
3.3.1 The accelerated regime	44
3.3.2 The wandering center of mass regime	45
3.3.3 The invariant regime	46
4 Conclusions and perspectives	47

A Stochastic Noise	50
B Numerical simulation of stochastic processes	53
Bibliography	55

List of Figures

1.1	A big flock composed of hundreds of birds.	1
1.2	Examples of swarming behaviour in large groups.	2
1.3	Graphic representation of the interaction regions determined by an euclidean (left) and topological (right) metric.	4
1.4	Ordered motion takes place for high density and small noise, $N = 300$. Image from [1].	6
1.5	Counterclockwise and double mills generated by the current model. Images taken from [17].	8
1.6	Unconditional flocking of a swarm of a hundred particles.	9
1.7	Small swarm guided by 5 leaders (red particles); the target is represented by the light blue triangle.	10
2.1	Crystalline pattern generated by 1000 particles, when only potential and friction terms govern the dynamics of the swarm. The center of mass is represented with the pink dot.	13
2.2	Potential function (blue line) with the two regions of repulsion (red) and attraction (green).	14
2.3	Representation of potential forces between two particles.	15
2.4	Center of mass velocity trends depending on different values of the alignment characteristic length. Only in this case the noise has been neglected in numerical simulations for the sake of clarity.	17
3.1	Graphical representation of the random initial placement of two particles.	29
3.2	Difference between $l_c = 10$ and $l_c = 10^3$ cases. The plot shows the alignment factors as distance functions in the weighted average process.	30
3.3	Center of mass modulus and x-velocity over time.	32
3.4	Series of images representing the evolution of the swarm configuration over time. The time step of each snapshot is reported. The pink dot represents the center of mass, while the light blue one is the "Alice" particle.	33

3.5	Center of mass x-displacement (left), and trajectories of the center of mass and of the "Alice" particle.	34
3.6	Numerical output for "Alice" position and x-velocity during the simulation.	34
3.7	Swarm center of mass velocity during a simulation. Comparison between analytical and numerical results in the case $l_c = 1000$	35
3.8	Alignment of the swarm after 9000 time steps. Initial evolution of center of mass and "Alice" trajectories.	35
3.9	The first two pictures represent the swarm configuration at the beginning and after 9000 time steps. The latter concern evolution of the x component of center of mass velocity and position over time.	36
3.10	"Alice" x-velocity and trajectories of center of mass and "Alice" particle.	37
3.11	Center of mass velocity and trajectories in case of zero initial mean velocity.	37
3.12	These pictures refer to the case without noise. The first two represent "Alice" particle velocity and displacement, while the latter show center of mass x-velocity and swarm final configuration.	38
3.13	Center of mass velocity and displacement evolution during the simulation. Again only the x-component is considered.	39
3.14	Evolution over time of the swarm configuration.	40
3.15	Center of mass and "Alice" particle x-velocity during a typical simulation with $l_c = 10$	41
3.16	Center of mass and "Alice" x-velocity evolution over time ($l_c = 1000$).	41
3.17	Snapshots of the spatial configuration of the swarm taken at different time steps ($l_c = 1000$).	42
3.18	Comparison between x-displacement of the center of mass for $l_c = 1000$ and $l_c = 10$	43
3.19	Variance and expected value of the swarm center of mass velocity from numerical simulations and analytical results. Semi-log plots. .	44
3.20	Velocity variance (semi-log plot) and expected value of the swarm center of mass. Comparison between analytical and numerical results.	45
3.21	Velocity variance and expected value of the swarm center of mass in case of invariant regime.	46
A.1	Trajectory of a single particle which dynamics is described by a 2D <i>Ornstein-Uhlenbeck</i> process. Images obtained after 10^4 time steps, $\beta = 0.5$, $m = 1$, $\sigma = 1$. The final position of the particle is represented with the light blue circle.	52
B.1	Discretized Brownian path after $5 \cdot 10^4$ iterations. The final position is represented with the cyan dot.	54

Chapter 1

Introduction on Swarm Models

1.1 Swarming behaviour in biology

One of the most beautiful and impressive natural phenomena, that has fascinated the observers since ancient times, is the spontaneous emerging of coherent behaviours in biological systems composed by a large number of interacting individuals. The ubiquity of such a phenomenon is an impressive and charming feature. Indeed, the



Figure 1.1: A big flock composed of hundreds of birds.

appearance of self-organization is observable at any spatial scale and in incredibly different contexts (see [5]). In this regard, I want to point out that there are several types of self-organizations. Some of these concern collective motions, while others appear as ordered structures or patterns.

There are plenty of examples of superficial textures of rare beauty, like the ones characterizing the leopard fur, butterfly wings or snakes or fish skin, and they belong also to the plant kingdom, just think about some wonderful flowers. We can observe similar patterns also at the microscopic scale, for instance in spatial patterns generated by cells following a chemoattractant, as reported in [29], or in segregation of two different cell populations, as described in [22]. This kind of sorting phenomena can be modelled through a continuum approach (diffusion-driven instability or "Turing instability"), or exploiting agent-based modelling (see [24]), but their analysis lays beyond the aim of the present work.

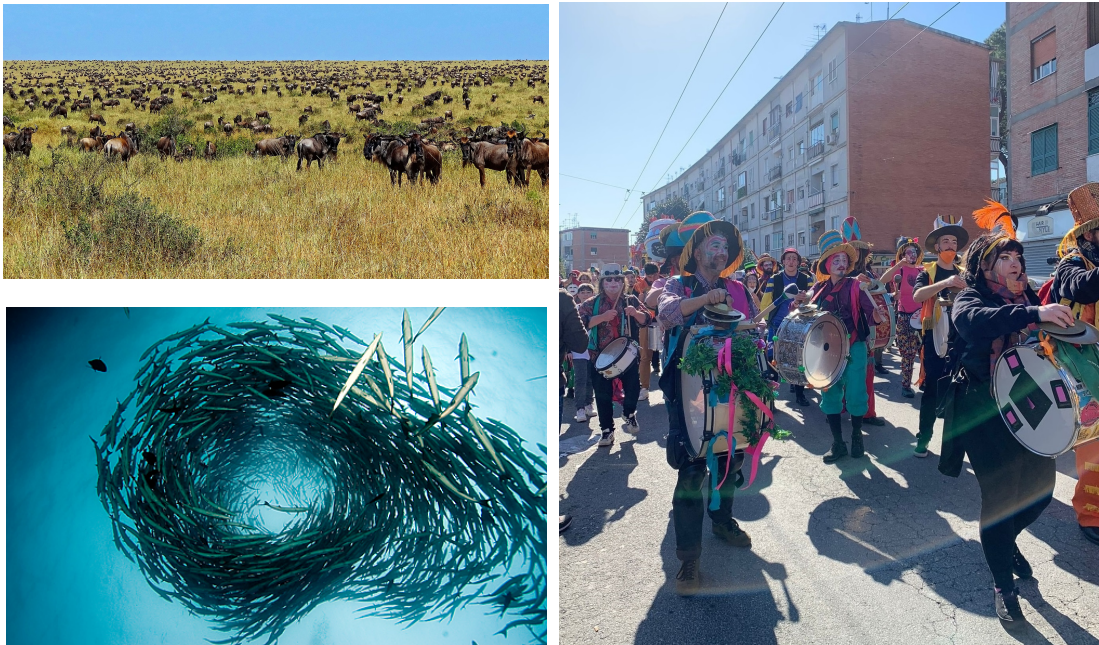


Figure 1.2: Examples of swarming behaviour in large groups.

Here I want to focus on *collective motions*, and in particular on *swarming* phenomenon. In this case coherent and synchronized behaviours appear in a large group of similarly sized individuals, and productive motion takes place even without the guide of leaders. It's also really interesting to underline that an individual behaves in a very different manner if it is within the swarm or if it is alone. Consequently, we can state that the individual dynamics is determined by the influence of the rest of the group. This kind of behaviours can be recognized, for instance,

in human crowds or in animal groups (fish schools, insect swarms, bird flocks or herds of herbivores), in which coherent behaviour emerges from an initial random configuration (see [15], [30] and [20]). Surprisingly, swarming behaviour has been observed also in the plant kingdom, specifically during the root system development, as shown in [18]. In this case, the system counts thousands of roots tips (which can be seen as the agents of the system), and swarming behaviour can appear as an efficient way to optimize resources or to explore the underground environment.

1.2 Different modelling approaches

There are different approaches in swarming modelling, depending on the considered spatial scale (see [17], "Part III: Human behavior and swarming", "Particle, Kinetic, and Hydrodynamic Models of Swarming", and [23]). A significant part of models reported in literature exploits a *microscopic* and *discrete* approach (*agent-based modelling*). In this case, the rules which define the single particle dynamics are directly set (for this reason they are also referred as "Lagrangian models", see [9]). Usually the governing equation is of *Langevin-type*, and so it has the form

$$m \frac{d\mathbf{v}}{dt} = -\beta \mathbf{v} + \boldsymbol{\xi}(t), \quad (1.1)$$

where $\boldsymbol{\xi}(t)$ is a noise term (*Wiener process*). Often this equation is solved in the overdamped (or low-Reynolds-number) regime. In this case, the equation of motion is reduced to a *force-velocity* relation, which defines the agent velocity as directly proportional to the acting forces, and so inertial effects are considered negligible. This overdamped models are applied to a wide range of biological situations: from the description of collective dynamics of a bee swarm (see [27], [28]), in which the information of the common direction is spread among individuals by one or more leaders (bee scouts), to collective cell migration (see [26] for an example of cancer cell migration, and [31] for chase-and-run migration in heterogeneous cell populations modelling), or to phase transition in biological tissues (see [11], in which the transition to collective movement is related to the cell density, and [25], that analyzes the jamming transition from a solid-like state to a liquid-like state in a dense cell environment).

In this kind of models a fundamental aspect is the metric type that governs the interactions amongst individuals, and so that defines shape and extension of the action area of a certain force. Most current studies consider an Euclidean metric-based neighborhood, for which the effect exerted by a neighbour depends only on the Euclidean distance between two individuals, and in this case, each influence region will be a circle or an annulus. On the other hand, there are evidences which suggest that in some natural contexts (for example in the case of a bird flock, as reported in [14]) the influence region depends on a topological metric,

and so, in other words, that each agent interacts in a certain manner with the k -closest neighbours. This metric type seems to guarantee significantly higher cohesion against external perturbations, typically predation. In Figure (1.3) a significant example is represented: in this case three different influence regions are considered depending on the acting force. The current models, as commonly assumed, counts three force terms, a repulsive, an attractive and an alignment one. In the topological case, right plot, it's easy to notice that, even if the repulsion and attraction regions continue to be defined via the euclidean distance between neighbours, the alignment area includes only the closest individuals with respect to the considered particle, and so it has not a predetermined shape. This first discrete

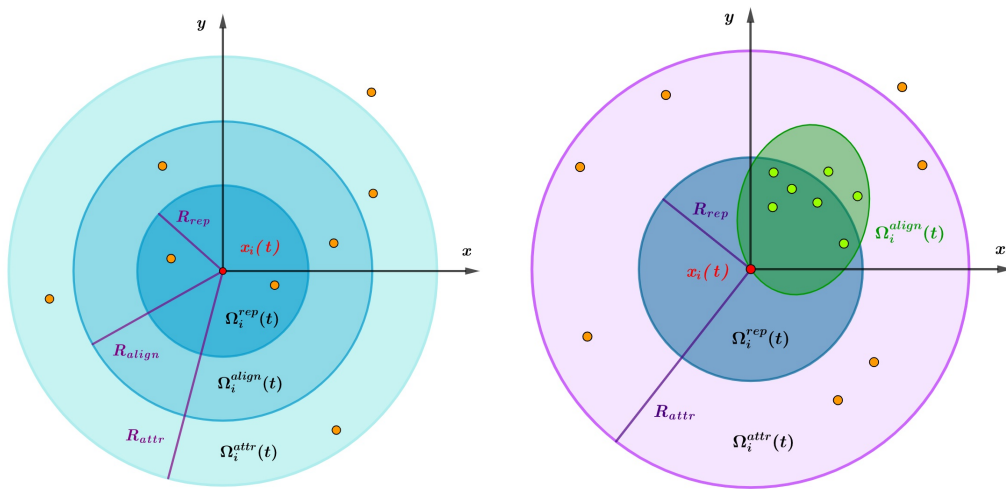


Figure 1.3: Graphic representation of the interaction regions determined by an euclidean (left) and topological (right) metric.

and microscopic approach is particularly suitable to describe the so called "*active matter*": a large particles ensemble, each of which is capable of active movement, due to some sort of internal metabolism. This peculiar feature makes this systems category being intrinsically out of thermal equilibrium, indeed, each agent continues to consume and dissipate energy. Often, for this reason, the system components are referred to as "*self-propelled particles*", because they are not merely prone to the environment-determined dynamics but, instead, they can show directed and persistent motion. This latter concept, and more generally the microscopic approach, is really useful in projecting and developing artificial swarms. Indeed, in the spirit of *biomimicry*, the understanding of natural collective motions can be translated into the modelling of the dynamics of drones swarm or micro-swimmer with many biomedical applications.

The other type of models assume a *macroscopic* point of view, and they exploits

a *continuum* approach (see as examples [17], [9], [16]). They are particularly useful when the number of individuals that compose the group is significantly large, as in case of insect swarms, fish schools or bacterial populations. Indeed, the solution of the resulting system of ordinary differential equations (ODEs), or of stochastic differential equations (SDEs), if random effects are considered, can be excessively expensive computationally speaking. These models rely on the definition of evolution equations, usually partial differential equations (PDEs) of reaction-advection-diffusion type, which describes macroscopic quantities such as the population density field $\rho(x, t)$ (they are also known as "Eulerian models", because they describe the local flux of individuals). Furthermore, they are based on conservation laws, such as conservation of mass and momentum, and on phenomenological assumptions (*constitutive relations*), often needed for the closure problem.

A link between the microscopic and the macroscopic point of view can be found through *kinetic models*, which describe how, from individual interactions among agents of the system, it is possible to derive collective behaviours in terms of overall quantities. The general idea, developed by Boltzmann during the 1870s in the context of kinetic theory of gases, consists in substituting the definition of the single particle dynamics with an aggregate statistical description of the entire system, on the basis of a single representative interaction between two generic particles.

Starting from the microscopic interaction rules, it is possible to derive an evolution equation for the probability density function $f = f(\mathbf{x}, \mathbf{v}, t) : \mathbb{R}^d \times \mathbb{R}^d \times [0, +\infty] \rightarrow \mathbb{R}$, in order to describe the system from a *mesoscopic* point of view ($d = 2, 3$ in order to observe spatial patterns). The equation takes the following form:

$$\left(\partial_t f + \mathbf{v} \cdot \nabla f\right)(\mathbf{x}, \mathbf{v}, t) = \mathcal{Q}(f, f)(\mathbf{x}, \mathbf{v}, t), \quad (1.2)$$

in which the first term represents a transport operator (distribution function f transported with velocity v by the freely moving particles), while the second term is the *interaction operator*. This latter term, which is a bilinear operator, accounts for the balance between gain and loss (in a statistical sense) of particles with velocity v in the unit time as a consequence of interactions ("collisions", indeed it is also known as *collision operator*, for the original theoretical context in which it has been developed). The previous expression is known as *Boltzmann-type* equation, and from a weak formulation of it, it's possible to calculate statistical moments considering a suitable physical *observable* (for example, $\varphi(v) = 1, \mathbf{v}, \mathbf{v}^2$). In this way, statistical moments are related to macroscopic local quantities, such as local density $\rho(x, t)$ and mean velocity field $\mathbf{u}(x, t)$, and we can then write continuum-like equations for the conservation of mass (*continuity equation*) and momentum (as reported in [17]).

1.3 Brief overview on existing particle models

There is a rich literature developed during the last years about modelling collective motions, which characterize the so called "*active matter*". In this context, a large number of agents interact each other and they are capable of self-motion in far from equilibrium conditions. There have been many different attempts to describe in mathematical terms these wonderful and surprising phenomena of self-organization, and in this section I want to briefly report some significant examples. They are of great interest, since each of them shows different mathematical approaches for describing a given characteristic of the observed phenomenon, and they focus on different aspects of the system dynamics (for example, rotating patterns or flocking). I'm particular interested in the way these models define the *alignment mechanism*, which is a fundamental aspect of the collective behaviour.

1.3.1 Vicsek model

One of the first models has been proposed by Tamás Vicsek and co-workers (see [1]), which attempted to insert this wonderful class of natural phenomena into a mathematical framework. They presented a simple model to investigate the emergence of self-ordered motion in systems of self-propelled particles, taking into account biological interactions via mathematical evolution rules. In their model particles have negligible size, and the point-like units move with constant speed modulus. At each time step they change their direction of motion in accordance with the average direction of other particles within a given distance r . Random effects are also taken into account adding a stochastic perturbation term to the direction evolution equation.



Figure 1.4: Ordered motion takes place for high density and small noise, $N = 300$. Image from [1].

In a typical simulation, N particles are randomly distributed throughout the domain with the same absolute velocity v and randomly distributed directions θ . Velocities $\{\mathbf{v}_i\}$ of the agents are determined simultaneously at each time step, and the position of the i -th particle is updated according to

$$\mathbf{x}_i(t+1) = \mathbf{x}_i(t) + \mathbf{v}_i(t)\Delta t. \quad (1.3)$$

The velocity at the following time step, $\mathbf{v}_i(t+1)$, is constructed in order to have modulus equal to v and a direction given by $\theta(t+1)$. This angle is obtained as

$$\theta_i(t+1) = \langle \theta(t) \rangle_r + \Delta\theta_i, \quad (1.4)$$

where $\langle \theta(t) \rangle_r$ denotes the average direction of particles contained within a circle of radius r centered in the i -th particle, and the term $\Delta\theta_i$ is a random perturbation, which value is extracted from a uniform probability distribution on the interval $[-\eta/2, \eta/2]$. It is interesting to note that also the velocity of the i -th particle is taken into account in the averaging process, while calculating the new direction. In a way, it is a manner for taking into consideration inertial effects, in the sense that $\mathbf{v}_i(t)$ affects $\mathbf{v}_i(t+1)$, but the dependence on the previous time step velocity is lost as the number of neighbours increases.

In this case, there are three parameters governing the dynamics of the system: η , the noise amplitude, ρ , the density of particles, and v the constant speed modulus, that expresses the distance covered by a particle during a time step. The authors emphasize that the most interesting regime is the one characterized by high density and low noise intensity, and in this condition a kinetic phase transition is observed: particles begin to move in the same spontaneously selected direction performing net displacement and so motion becomes ordered on a macroscopic scale.

This simple model is capable of reproducing collective behaviour, as rotation or flocking, and it provides fundamental insights on a wide range of biological phenomena involving clustering and migration.

1.3.2 D’Orsogna-Bertozzi model

The model described in the following has been proposed by D’Orsogna and Bertozzi in 2006 (see [10] for more information), and it considers self-propelled particles subjected to frictional and attractive/repulsive forces due to the presence of neighbours. These latter, are modelled via a Morse potential, which is a pairwise and radial function. It’s remarkable that they also provided an analysis of stability and morphology of the swarm starting from the shape of the two-body interaction. In fact, as they stated, a fundamental aspect of swarming dynamics is the understanding of how particles rearrange into space when their number increases. The agents can both organize into a crystalline-like structure with a well defined spacing, or collapse overlapping one over the other. Considering results from statistical mechanics, they identified regions of the phase diagram of Morse potential characterized by a stable or a catastrophic regime. In the present model, the dynamics of the N identical particles is defined by the following equations of motion:

$$\begin{cases} \frac{d\mathbf{x}_i}{dt} = \mathbf{v}_i \\ \frac{d\mathbf{v}_i}{dt} = (\alpha - \beta|\mathbf{v}_i|^2)\mathbf{v}_i - \frac{1}{N} \sum_{j \neq i} \nabla U(|\mathbf{x}_i - \mathbf{x}_j|), \end{cases} \quad (1.5)$$

where $U : \mathbb{R}^d \rightarrow \mathbb{R}$ is the Morse potential, which accounts for short-range repulsion and long-range attraction. Here all agents have the same size, and so unitary mass

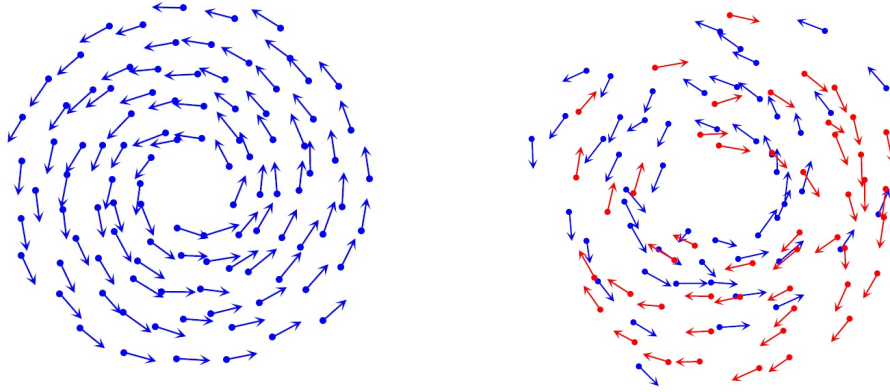


Figure 1.5: Counterclockwise and double mills generated by the current model. Images taken from [17].

has been considered. The potential U has the following mathematical expression:

$$U(x) = k(|x|), \quad k(r) = -C_A e^{-\frac{r}{l_A}} + C_R e^{-\frac{r}{l_R}}, \quad (1.6)$$

where C_A, C_R and l_A, l_R are respectively the intensities and the typical lengths of attraction and repulsion. Moreover, α parameter models the *self-propulsion* of individuals, while β represents the friction contribution, and the balance between these two terms leads to the asymptotic speed $|\mathbf{v}| = \sqrt{\alpha/\beta}$.

As a result of the chosen microscopic dynamics, the model is capable to simulate formation of stable particle vortices with one or two simultaneous directions of motion. The emergence of this structure, however, can depend also on boundary conditions and domain shape, as reported in [2].

In the cited article, the authors underline how both the stable and catastrophic regimes can interestingly have proper applications. The first can describe bacterial colonies dynamics (see for example *Myxococcus xanthus* myxobacteria), in which formation of rotating structures with increasing density and compenetration between cells has been observed. The second one, instead, can be applied in modelling artificial swarms for which an adequate spacing amongst system components is desirable, in order to avoid collisions.

1.3.3 Cucker-Smale model

This model has been proposed by Cucker and Smale (see [12] and [17]) and, as a fundamental feature, it takes into account only an *alignment* mechanism in defining the microscopic dynamics of the single particle. It determines the motion of the particles averaging the relative velocities of neighbours. In this case, the influence

of the single individual on the alignment process is weighted by its relative distance, and so closer neighbours exert greater influence than further ones. I think it is an important assumption and it deserves particular attention: indeed, assuming that all individuals contribute in the same way to the average velocity of the i -th particle (even if only inside a prescribed area, as in the Vicsek model), can be a too strong approximation, depending on the biological context of interest. Then we can present the governing equations of the model:

$$\begin{cases} \frac{d\mathbf{x}_i}{dt} = \mathbf{v}_i \\ \frac{d\mathbf{v}_i}{dt} = \frac{1}{N} \sum_{j=1}^N H(|\mathbf{x}_i - \mathbf{x}_j|)(\mathbf{v}_j - \mathbf{v}_i), \end{cases} \quad (1.7)$$

where the function H accounts for the weighting process based on mutual distance between particles. It has the following form

$$H(\mathbf{x}) = a(|\mathbf{x}|), \quad a(r) = \frac{K}{(\sigma^2 + |r|^2)^\gamma}, \quad (1.8)$$

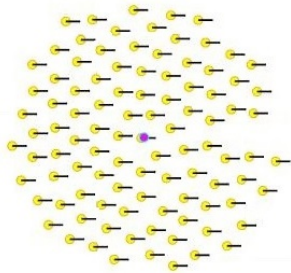


Figure 1.6: Unconditional flocking of a swarm of a hundred particles.

tendency to align, moving with the same mean velocity, and to arrange into a group with fixed mutual distances, but not necessarily in a crystalline-type pattern. This configuration emerges from the internal reorganization of the swarm guided by the alignment process. This observation allow us to state that the presence of the alignment term is of crucial importance in determining net motion. Here I want to highlight that the two last reported models show a deterministic dynamics, but it can be verified that they are stable also in presence of small intensity noise fluctuations, as reported by the authors.

in which K, σ and γ are positive parameters that govern the different model regimes. The function H it is also defined as *communication rate*, since it modulates the intensity of the effect that a certain individual exerts on another one. Actually we can state that if the influence is negligible, the two particles are not communicating, or interacting. One of the possible collective behaviours simulated by the present model is the so called "*unconditional flocking*". In such a situation, particles exhibit the

1.3.4 Swarming models with leaders

The three models presented above simulate the spontaneous reorganization of a swarm into defined patterns, as a result of the microscopic individual dynamics. The emergence of coherent behaviour can be determined by an alignment mechanism (Vicsek and Cucker-Smale models) or thorough the concurrent presence of a frictional and a potential term, which accounts for social stimuli of repulsion and attraction. In these cases all the particles have same size and same role inside the group, indeed they are interchangeable, and they spontaneously organize without any information from the outside. This eventual external stimulus could model the effect of a chemical gradient (chemotaxis), of an electromagnetic field, or of a different stiffness of the substrate on which particles are moving (durotaxis). Because of this lack of external information, the productive movement observable in swarming simulations from the previous models has random direction.

In other natural phenomena it is observed that the movement of the swarm is guided by leaders, and they are characterized by a different dynamics from other group members. In fact, the information brought by leaders has to be always available, in order to spread it

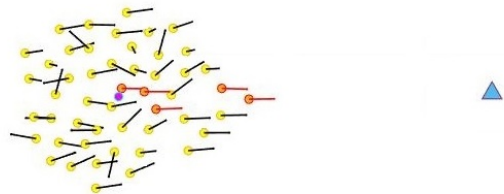


Figure 1.7: Small swarm guided by 5 leaders (red particles); the target is represented by the light blue triangle.

to the rest of individuals and to guide them towards a target position. We can recognize a wide variety of swarming phenomena guided by multiple leaders. For example, in cellular sheet migration during wound healing, "leader cells" situated at the front edge guide the collective motion towards the cell-free space (see [22]). Another interesting case, it's the migration of bees when a colony splits into two (or more) independent ensembles because of the birth of a new queen. During swarming, after have identified a suitable nest site (there is a "democratic" decision between the explorers, that communicate each other possible locations via the curious *waggle dance*), worker-bees with the old queen are guided by scouts towards the new destination. It is estimated that less than 5% of the bees are informed about the right direction to follow, but, however, the entire swarm is capable of net motion and coherent behaviour. There are some mathematical models (see [19] and [28] as examples) that simulate the honeybee swarming guided by scouts. Interestingly, It has been studied that the larger the group, the smaller the portion of informed individuals needed to reach the target destination (see [7]), and that beyond a certain threshold there is not appreciable benefit in increasing the number

of leaders. For large groups of social animals, such as honeybee colonies, there are likely some costs about recruiting more explorers, for example in energetic or metabolic terms (just think how, if the entire community were considered as a whole, a greater number of informed individuals would result in an increased global consumption of natural resources); so, reaching the best trade-off between explorers number and efficiency of the migration is of fundamental importance, and it can be seen as the result of an evolutionary adaptation.

Chapter 2

Mathematical Model

2.1 Introduction to the current model

In this section I want to present the mathematical model we developed to simulate the collective dynamics of a swarm of self-propelled particles. I studied many different examples, and I constructed the current model taking various "mathematical ingredients" from different sources (see, for instance, [3] and [8]), on the basis of the assumptions we made and on biological reasons. Unlike most of cases, we solved the particle dynamics as a *stochastic process*. Consequently, our motion equations assume the form of SDEs, unlike ODEs or PDEs commonly used. This allowed us to perform a statistical analysis in order to investigate physical quantities describing the overall behaviour of the swarm, such as the expected value and the variance of the center of mass velocity and position.

We identify the i -th agent with the couple $(\mathbf{x}_i, \mathbf{v}_i) \in \mathbb{R}^4$, where $\mathbf{x}_i = (x_i, y_i)$ and $\mathbf{v}_i = (v_i, u_i)$, and so we represent it as a material point in \mathbb{R}^2 considering its size to be negligible. Moreover, each particle of the swarm has the same mass, so that the total mass of the system is equal to $M = Nm$, with N number of the swarm components. In our model the microscopic dynamics of the i -th particle is governed by the following *Langevin-type* equation:

$$\begin{cases} d\mathbf{x}_i = \mathbf{v}_i dt \\ m d\mathbf{v}_i = -\beta \mathbf{v}_i dt - \nabla U_i dt + \mathbf{f}_i^A dt + \sigma d\mathbf{W}_t^i \end{cases} \quad \text{with } i = 1, 2, \dots, N. \quad (2.1)$$

The first term on the right side of the second equation represents a frictional force, proportional to the particle velocity and with damping coefficient $[\beta] = [M] \cdot [T]^{-1}$; the second term, that is the gradient of a pairwise radial potential (*Morse-type* potential), accounts for social stimuli of repulsion and attraction (as done, for example, in [3] and [10]); the third one defines the alignment contribution, and the last one is a stochastic noise whose intensity is modulated by the constant σ (from

now on we consider $\sigma = 1$, without loss of generality). Returning to the potential term, the repulsive effect ensures a minimum space between particles (avoiding compenetrations and collisions between neighbours), while the attractive one models the tendency of an individual to maintain a connection with the swarm (it can simulate the desire of social animals to remain close to the rest of the group, or a mechanical bond between particles, as in a cell culture). The Morse potential has the following mathematical expression:

$$U = \sum_{j \neq i}^{N-1} C_a e^{-\frac{|\mathbf{x}_j - \mathbf{x}_i|}{l_a}} - C_r e^{-\frac{|\mathbf{x}_j - \mathbf{x}_i|}{l_r}}, \quad (2.2)$$

in which parameters C_a and C_r determines the strength of the interactions and l_a and l_r are respectively the attraction and the repulsion typical lengths. The potential force is given as the negative derivative of the Morse potential, so:

$$-\nabla U(x, y) = \sum_{j \neq i}^{N-1} \left(C_a \frac{e^{-\frac{|\mathbf{x}_{ij}|}{l_a}}}{|\mathbf{x}_{ij}| l_a} - C_r \frac{e^{-\frac{|\mathbf{x}_{ij}|}{l_r}}}{|\mathbf{x}_{ij}| l_r} \right) \mathbf{x}_{ij} + \left(C_a \frac{e^{-\frac{|\mathbf{x}_{ij}|}{l_a}}}{|\mathbf{x}_{ij}| l_a} - C_r \frac{e^{-\frac{|\mathbf{x}_{ij}|}{l_r}}}{|\mathbf{x}_{ij}| l_r} \right) \mathbf{y}_{ij}. \quad (2.3)$$

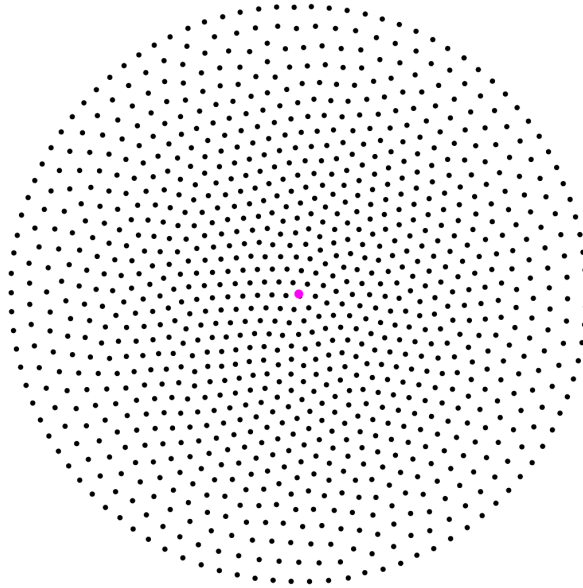


Figure 2.1: Crystalline pattern generated by 1000 particles, when only potential and friction terms govern the dynamics of the swarm. The center of mass is represented with the pink dot.

Here, $\mathbf{x}_{ij} = \mathbf{x}_j - \mathbf{x}_i$ is the difference between the i -th particle position and the j -th one, and from now on we will adopt this formalism. It has been observed that most relevant conditions for biological applications take place in case of long-range attraction and short-range repulsion, and they are obtained by setting $C = C_r/C_a > 1$ and $l = l_r/l_a < 1$ (see [17]). We can also observe that the potential term accounts for the internal spacing of the swarm, and so it determines mutual distances between particles. In our case the potential parameters lead to a catastrophic regime, as defined in [10], and so the diameter of the swarm doesn't depend on the number of particles. Moreover, as reported in [3], numerical simulations revealed that the swarm reaches a constant size increasing the N value. We can thus state that in our model the swarm diameter is only a function of the potential parameters, and so $d = f(C_r/C_a, l_r/l_a) = f(C, l)$.

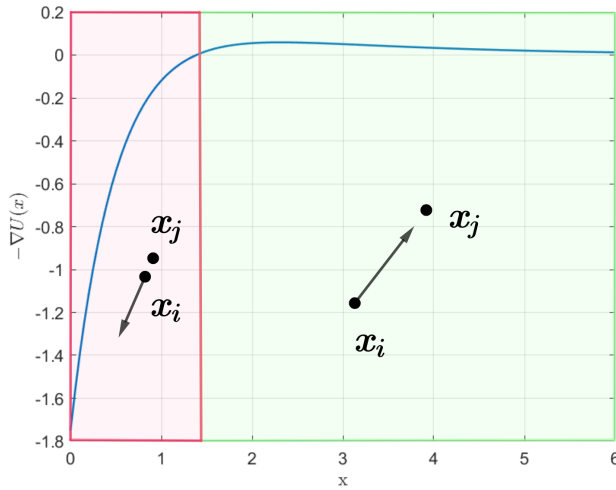


Figure 2.2: Potential function (blue line) with the two regions of repulsion (red) and attraction (green).

It has the following mathematical expression:

$$\mathbf{f}_i^A = \frac{\alpha}{N-1} \sum_{j \neq i}^{N-1} \mathbf{v}_j e^{-\frac{|\mathbf{x}_{ij}|}{l_c}} \quad (2.4)$$

where l_c is again a characteristic length, and the α parameter modulates the intensity of the alignment interaction. Moreover, I want to briefly discuss the choice of the current alignment term. Considering a given particle, the alignment term basically consists of the average of neighbours velocity weighted by the mutual distances (which are the argument of the negative exponential function). In our model we assumed an Euclidean metric for the definition of the alignment mechanism, but without setting bounded regions of action; this choice is explained by considering

the fast decay of the exponential function, which guarantees that far individuals do not affect the dynamics of the i -th particle, since in this case the velocity multiplying factor in the average process is near zero. We didn't implement a topological metric since it requires that only the k -closest neighbours are involved in the alignment process (for example, 6 to 7 in case of bird flock, see [14]), and so it can not account for the influence of several neighbours in case of high density swarms. The i -th particle definitely perceives strongly the closest neighbours, but, at the same time, it should also be influenced by the presence of a large number of group members beyond them.

Finally, the last term is a stochastic fluctuation, that plays the role of a perturbation of the deterministic dynamics. Indeed, since we are modelling the behaviour of active particles, capable of self-propulsion, we have to give them some sort of "free will", in order to allow the possibility of not merely following the social rules of the system (such as repulsion/attraction effects or the incentive to align with neighbours). Specifically, the noise term is modelled as a *standard Brownian motion*, that is a random process $\mathbf{W}^i(t)$ that depends continuously on time, and its increments are normally distributed as $d\mathbf{W}_t^i = \sqrt{dt} \boldsymbol{\xi}$, where $\boldsymbol{\xi}$ is a vector random variable with normal distribution. I want to emphasize that the random terms for each particle are independent of each other.

2.2 Swarm center of mass equations

In the previous section I presented the model we developed, briefly focusing on each term that appears in the *Langevin* equation, and describing their main characteristics and the underlying modelling reasons.

Now we derive the equations for the center of mass velocity and position, which define the dynamics of the swarm, in a manner similar to the one followed in [8]. Summing the evolution equations for all the particles, we obtain

$$\sum_{i=1}^N m d\mathbf{v}_i = \sum_{i=1}^N -\beta \mathbf{v}_i dt - \nabla U_i dt + \mathbf{f}_i^A dt + d\mathbf{W}_t^i. \quad (2.5)$$

Now, we can notice that $\sum_{i=1}^N \mathbf{v}_i = N\mathbf{V}$, where \mathbf{V} is the velocity of the swarm center of mass, and the same observation holds also for the inertial term on the left. Instead, the summation of all the potential forces lead to cancel the corresponding terms, since, as internal forces of the system, they balance each other. I want to give a proof of this result considering two particles, but obviously it can be extended to an arbitrary

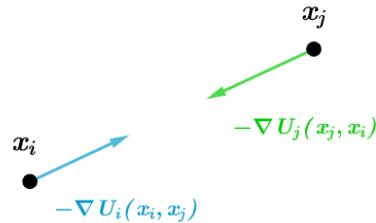


Figure 2.3: Representation of potential forces between two particles.

large number of them. Let's start considering the potential force acting on the i -th particle:

$$-\nabla U_i(\mathbf{x}_i, \mathbf{x}_j) = C_a e^{-\frac{|\mathbf{x}_{ij}|}{l_a}} \frac{\mathbf{x}_{ij}}{l_a |\mathbf{x}_{ij}|} - C_r e^{-\frac{|\mathbf{x}_{ij}|}{l_r}} \frac{\mathbf{x}_{ij}}{l_r |\mathbf{x}_{ij}|}, \quad (2.6)$$

and it's clear that, if the attractive effect overcomes the repulsive one, the i -th particle will be affected only by an attractive force directed as \mathbf{x}_{ij} . We can also write the potential force acting on the j -th particle, and it is:

$$-\nabla U_j(\mathbf{x}_j, \mathbf{x}_i) = C_a e^{-\frac{|\mathbf{x}_{ij}|}{l_a}} \frac{\mathbf{x}_{ji}}{l_a |\mathbf{x}_{ij}|} - C_r e^{-\frac{|\mathbf{x}_{ij}|}{l_r}} \frac{\mathbf{x}_{ji}}{l_r |\mathbf{x}_{ij}|}. \quad (2.7)$$

Now, observing that the two potential forces have the same modulus but opposite direction, since $\mathbf{x}_{ij} = -\mathbf{x}_{ji}$, we obtain

$$\nabla U_i(\mathbf{x}_i, \mathbf{x}_j) + \nabla U_j(\mathbf{x}_j, \mathbf{x}_i) = 0. \quad (2.8)$$

This balance between internal forces of the swarm holds for any number of particles, since considering the single couple we always observe the balance of potential interactions.

Then I want to focus on the alignment term. Considering the limit $l_c \rightarrow \infty$, the exponential factor tends to 1, and so the velocities of all the neighbours are weighted in the same way. This assumption is justified if $l_c \gg \max(|\mathbf{x}_{ij}|)$, and it can model some sort of mechanical connection between particles, so that also the velocity of far agents affects the dynamics of a given particle. In our case numerical simulations show that the constant diameter reached by the swarm $d = \max(|\mathbf{x}_{ij}|) \approx 4$. So, we get the following expression for the alignment term:

$$\mathbf{f}_i^A = \frac{\alpha}{N-1} \sum_{i=1}^N \sum_{j \neq i}^{N-1} \mathbf{v}_j = \frac{\alpha}{N-1} N(N-1) \mathbf{V} = \alpha N \mathbf{V}, \quad (2.9)$$

where again \mathbf{V} is the velocity of the swarm center of mass. Finally we have to rearrange also the noise term. We know from the probability theory that by summing two independent and normally distributed random variables, such that

$$\begin{aligned} X &\sim \mathcal{N}(\mu_x, \sigma_x^2) \\ Y &\sim \mathcal{N}(\mu_y, \sigma_y^2), \end{aligned}$$

we get another random variable, defined as

$$X + Y \stackrel{d}{=} Z \sim \mathcal{N}(\mu_x + \mu_y, \sigma_x^2 + \sigma_y^2).$$

In fact the Gaussian distribution is a *stable* probability density function, and this means that a linear combination of two random Gaussian variables is again a

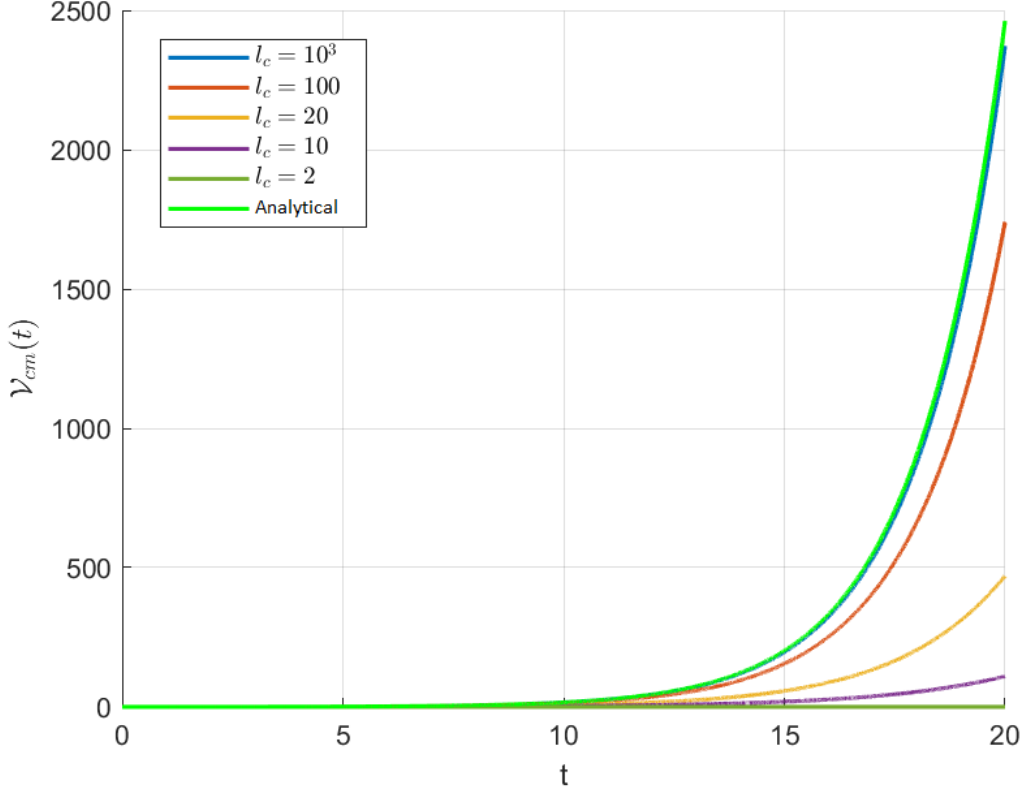


Figure 2.4: Center of mass velocity trends depending on different values of the alignment characteristic length. Only in this case the noise has been neglected in numerical simulations for the sake of clarity.

random Gaussian variable. Therefore, the summation of N noise terms, which are normally distributed, gives us

$$\sum_{i=1}^N d\mathbf{W}_t^i \stackrel{\mathbf{d}}{=} \sqrt{N}d\tilde{\mathbf{W}}_t, \quad d\tilde{\mathbf{W}}_t \sim \mathcal{N}(0,1). \quad (2.10)$$

Then, collecting these last results, we can write the center of mass velocity evolution equation as

$$mNd\mathbf{V} = -\beta N\mathbf{V}dt + \alpha N\mathbf{V}dt + \sqrt{N}d\tilde{\mathbf{W}}_t, \quad (2.11)$$

and, dividing by N , we finally obtain:

$$md\mathbf{V} = (\alpha - \beta)\mathbf{V}dt + \frac{1}{\sqrt{N}}d\tilde{\mathbf{W}}_t. \quad (2.12)$$

Hereinafter I will drop the tilde symbol for the sake of clarity. Results of simulations performed with different alignment characteristic lengths l_c are reported in Figure

(2.4). Numerical results have been compared with the analytical prediction in order to test the model behaviour. Rather than being a physical quantity of the system, the parameter l_c models the discrepancy between a standard average procedure and the one weighted by the exponential factor. So, the smaller the value of l_c , the greater the divergence between the standard and the weighted average processes. In other words, the lower the value of l_c , the stronger the influence of the closest neighbours on the alignment contribution in the dynamics of the i -th particle.

2.3 Statistical analysis of the center of mass equations

In this section I report the calculations about expected value and variance of the swarm center of mass velocity and position (here we considered only one dimensional analysis, but it holds for each of the spatial components). I also emphasize how different regimes, depending on different parameters configurations, lead to strongly diverging results. I begin reporting results about the statistical analysis of the center of mass velocity. Consequently, starting from them, we derive also analogous results for the center of mass position.

2.3.1 Swarm center of mass velocity equation

Let's begin writing the one-dimensional form of *Langevin equation* (2.12) for the center of mass velocity:

$$mdV = (\alpha - \beta)Vdt + \frac{1}{\sqrt{N}}dW_t, \quad (2.13)$$

in which the last noise term comes from the sum of all the Gaussian noise increments applied to the dynamics of each single particle, as introduced in the previous section. We can rearrange the equation in order to obtain an explicit solution for V :

$$dV - \frac{(\alpha - \beta)}{m}Vdt = \frac{1}{m\sqrt{N}}dW_t, \quad (2.14)$$

and, multiplying both sides by the exponential term $e^{-\frac{(\alpha-\beta)}{m}t}$ and integrating,

$$\int d(e^{-\frac{(\alpha-\beta)}{m}t}V) = \int \frac{e^{-\frac{(\alpha-\beta)}{m}t}}{m\sqrt{N}}dW_t, \quad (2.15)$$

we get

$$e^{-\frac{(\alpha-\beta)}{m}t}V = V_0 + \int_0^t \frac{e^{-\frac{(\alpha-\beta)}{m}s}}{m\sqrt{N}}dW_s, \quad (2.16)$$

and finally,

$$V = V_0 e^{\frac{(\alpha-\beta)}{m}t} + \frac{1}{m\sqrt{N}} \int_0^t e^{\frac{(\alpha-\beta)}{m}(t-s)} dW_s. \quad (2.17)$$

In this last equation V_0 is a random variable with standard Gaussian distribution, accounting for the initial velocity random configuration of the swarm, and the last term is a stochastic integral. Because the integrand is smooth in time all interpretations of the stochastic integral are equivalent to the *Itô*'s one, and so it is actually an *Itô* integral. The next step is to evaluate the expected value for each term in the equation:

$$\mathbb{E}[V] = \mathbb{E}[V_0] e^{\frac{(\alpha-\beta)}{m}t} + \underbrace{\mathbb{E}\left[\frac{1}{m\sqrt{N}} \int_0^t e^{\frac{(\alpha-\beta)}{m}(t-s)} dW_s\right]}_{=0 \text{ for Itô integral properties}}. \quad (2.18)$$

Here we considered *Itô integral* properties (see [21], chapter 3, section 3.2, Theorem 3.2.1). Now, we can calculate the variance of the swarm center of mass velocity:

$$\begin{aligned} \mathbb{E}[(V - \mathbb{E}[V])^2] &= \mathbb{E}\left[\left((V_0 - \mathbb{E}[V_0])e^{\frac{(\alpha-\beta)}{m}t} + \frac{1}{m\sqrt{N}} \int_0^t e^{-\frac{(\alpha-\beta)}{m}(t-s)} dW_s\right)^2\right] \\ &= \mathbb{E}\left[(V_0 - \mathbb{E}[V_0])^2 e^{\frac{2(\alpha-\beta)}{m}t}\right] + \mathbb{E}\left[\left(\frac{1}{m\sqrt{N}} \int_0^t e^{\frac{(\alpha-\beta)}{m}(t-s)} dW_s\right)^2\right] + \\ &\quad + \underbrace{\mathbb{E}\left[2(V_0 - \mathbb{E}[V_0])\frac{1}{m\sqrt{N}} \int_0^t e^{\frac{(\alpha-\beta)}{m}(t-s)} dW_s\right]}_{=0 \text{ for Itô integral properties and independence between } V_0 \text{ and } W_t}. \end{aligned} \quad (2.19)$$

Exploiting the *Itô isometry* reported below (see [21]), which is stated for a general function $f(s)$ which is adapted to the filtration generated by the *Wiener process* W_s (i.e. it can not depend on the future)

$$\mathbb{E}\left[\left(\int_0^t f(s) dW_s\right)^2\right] = \int_0^t (f(s))^2 dt, \quad (2.20)$$

we finally obtain

$$\begin{aligned} \text{Var}(V) &= \text{Var}(V_0) e^{\frac{2(\alpha-\beta)}{m}t} + \frac{1}{m^2 N} \int_0^t e^{\frac{2(\alpha-\beta)}{m}(t-s)} ds \\ &= \text{Var}(V_0) e^{\frac{2(\alpha-\beta)}{m}t} + \frac{1}{2mN(\alpha-\beta)} \left[e^{\frac{2(\alpha-\beta)}{m}t} - 1 \right] \\ &= \left[\text{Var}(V_0) + \frac{1}{2mN(\alpha-\beta)} \left(1 - e^{-\frac{2(\alpha-\beta)}{m}t} \right) \right] e^{\frac{2(\alpha-\beta)}{m}t}. \end{aligned} \quad (2.21)$$

We can now analyze the different regimes depending on combinations of parameters α and β . Considering the case $\alpha > \beta$ we observe that, after a transient,

$$\text{Var}(V) = \left[\text{Var}(V_0) + \frac{1}{2mN(\alpha - \beta)} \right] e^{\frac{2(\alpha-\beta)t}{m}}, \quad (2.22)$$

and so the variance of the swarm center of mass velocity increases exponentially, and it means that its values will show a strongly higher dispersion over time. Note that for increasing particles mass and number of swarm components, the second terms becomes negligible, and so the only contribution comes from the initial velocity variance. A similar condition is observable also for the expected value:

$$\mathbb{E}[V] = \mathbb{E}[V_0] e^{\frac{(\alpha-\beta)t}{m}}, \quad (2.23)$$

the mean velocity again grows exponentially, even if the exponent is lower than the one of the previous case.

In the case $\alpha < \beta$, we observe the opposite situation, indeed, for a long time the variance reaches a constant value and the expected value approaches zero:

$$\text{Var}(V) = \frac{1}{2mN(\beta - \alpha)}, \quad (2.24)$$

$$\mathbb{E}[V] = 0. \quad (2.25)$$

The last case $\alpha = \beta$ leads to:

$$\mathbb{E}[V] = \mathbb{E}[V_0], \quad (2.26)$$

and so, the expected value of the swarm velocity is equal to the initial expected value; for what concerns the variance, from the first row of equation (2.21) we have that it grows linearly in time

$$\text{Var}(V) = \text{Var}(V_0) + \frac{1}{m^2N}t. \quad (2.27)$$

2.3.2 Swarm center of mass position equation

Here I will follow a similar approach to the one presented above, but I'm interested in analyzing the different diffusion regimes characterizing the swarm center of mass dynamics. It's important to underline that, since we made the assumption $l_c \gg \max(|\mathbf{x}_{ij}|)$, in order to derive the center of mass velocity equation, all the particles will move as a whole, and the center of mass motion is representative of the entire swarm. Let's consider again the equation for the velocity of the center of mass:

$$V = V_0 e^{\frac{(\alpha-\beta)t}{m}} + \frac{1}{m\sqrt{N}} \int_0^t e^{\frac{(\alpha-\beta)(t-s)}{m}} dW_s, \quad (2.28)$$

and, by integration, we obtain

$$X = X_0 + \frac{m}{(\alpha - \beta)} V_0 \left[e^{\frac{(\alpha - \beta)}{m} t} - 1 \right] + \underbrace{\frac{1}{m\sqrt{N}} \int_0^t \int_0^\tau e^{\frac{(\alpha - \beta)}{m}(\tau - s)} dW_s d\tau}_{(\clubsuit)}. \quad (2.29)$$

Now, in order to rewrite the last term in a simpler way, we exploit the integration by parts $\int u dv = uv - \int v du$ following the procedure presented in [6]. In our case, it becomes:

$$\begin{aligned} dv &= e^{\frac{(\alpha - \beta)}{m} \tau} d\tau & du &= e^{\frac{(\alpha - \beta)}{m}(-\tau)} dW_\tau \\ v &= \int_0^t e^{\frac{(\alpha - \beta)}{m} \bar{\tau}} d\bar{\tau} & u &= \int_0^t e^{\frac{(\alpha - \beta)}{m}(-s)} dW_s, \end{aligned}$$

and so, we get the expression

$$(\clubsuit) = \underbrace{\frac{1}{m\sqrt{N}} \int_0^t e^{\frac{(\alpha - \beta)}{m}(-s)} dW_s \int_0^t e^{\frac{(\alpha - \beta)}{m} \bar{\tau}} d\bar{\tau}}_{(i)} - \underbrace{\frac{1}{m\sqrt{N}} \int_0^t \int_0^\tau e^{\frac{(\alpha - \beta)}{m} \bar{\tau}} e^{\frac{(\alpha - \beta)}{m}(-\tau)} dW_\tau d\bar{\tau}}_{(ii)}, \quad (2.30)$$

in which we can rearrange the two terms (i) and (ii) in the following way:

$$\begin{aligned} (i) &= \frac{m}{(\alpha - \beta)} \left[e^{\frac{(\alpha - \beta)}{m} t} - 1 \right] \frac{1}{m\sqrt{N}} \int_0^t e^{\frac{(\alpha - \beta)}{m}(-s)} dW_s \\ &= \frac{1}{(\alpha - \beta)\sqrt{N}} e^{\frac{(\alpha - \beta)}{m} t} \int_0^t e^{-\frac{(\alpha - \beta)}{m} s} dW_s - \frac{1}{(\alpha - \beta)\sqrt{N}} \int_0^t e^{-\frac{(\alpha - \beta)}{m} s} dW_s \\ (ii) &= -\frac{1}{m\sqrt{N}} \int_0^t \frac{m}{(\alpha - \beta)} \left[e^{\frac{(\alpha - \beta)}{m} \tau} - 1 \right] e^{\frac{(\alpha - \beta)}{m}(-\tau)} dW_\tau \\ &= -\frac{1}{\sqrt{N}(\alpha - \beta)} \int_0^t \left[\underbrace{e^{\frac{(\alpha - \beta)}{m}(\tau - \tau)}}_{=1} - e^{-\frac{(\alpha - \beta)}{m}(\tau)} \right] dW_\tau \\ &\stackrel{(\tau \rightarrow s)}{=} \frac{1}{\sqrt{N}(\alpha - \beta)} \int_0^t e^{-\frac{(\alpha - \beta)}{m} s} dW_s - \frac{1}{\sqrt{N}(\alpha - \beta)} \int_0^t 1 dW_s. \end{aligned}$$

Finally, after noticing that there are two terms with opposite sign, we can rewrite the expression (2.30) as

$$(\clubsuit) = \frac{1}{(\alpha - \beta)\sqrt{N}} e^{\frac{(\alpha - \beta)}{m} t} \int_0^t e^{-\frac{(\alpha - \beta)}{m} s} dW_s - \frac{1}{(\alpha - \beta)\sqrt{N}} \int_0^t 1 dW_s. \quad (2.31)$$

Therefore the swarm center of mass position equation (2.29) takes the form

$$X = X_0 + \frac{m}{(\alpha - \beta)} V_0 [e^{\frac{(\alpha - \beta)}{m} t} - 1] + \frac{1}{(\alpha - \beta) \sqrt{N}} \left[e^{\frac{(\alpha - \beta)}{m} t} \int_0^t e^{-\frac{(\alpha - \beta)}{m} s} dW_s - \int_0^t 1 dW_s \right]. \quad (2.32)$$

Now, as we have done in the previous section, the next step will be to calculate the expected value of the X variable, and so of each term at the right side of the equals, because of the linearity of the operator. Consequently we have:

$$\mathbb{E}[X] = \mathbb{E}[X_0] + \frac{m}{(\alpha - \beta)} \left[e^{\frac{(\alpha - \beta)}{m} t} - 1 \right] \mathbb{E}[V_0], \quad (2.33)$$

since the last two terms of the above equation has zero expected value because of *Itô integral* properties (as reported previously). Then, we have all the elements to write the variance expression as follow:

$$\begin{aligned} \text{Var}(X) &= \mathbb{E}[(X - \mathbb{E}[X])^2] \\ &= \mathbb{E} \left[\left((X_0 - \mathbb{E}[X_0]) + \frac{m}{(\alpha - \beta)} [e^{\frac{(\alpha - \beta)}{m} t} - 1] (V_0 - \mathbb{E}[V_0]) + \right. \right. \\ &\quad \left. \left. + \frac{1}{(\alpha - \beta) \sqrt{N}} \left(e^{\frac{(\alpha - \beta)}{m} t} \int_0^t e^{-\frac{(\alpha - \beta)}{m} s} dW_s - \int_0^t 1 dW_s \right) \right)^2 \right]. \end{aligned} \quad (2.34)$$

Here we observe that all the mixed terms are equal to zero because of the independence between X_0 , V_0 and the *Wiener process* W_t , and again because of the *Itô integral* properties. Indeed the *covariance* of two random variable is defined as:

$$\text{Cov}(X, Y) = \mathbb{E}[(X - \mathbb{E}[X])(Y - \mathbb{E}[Y])] = \mathbb{E}[XY] - \mathbb{E}[X]\mathbb{E}[Y], \quad (2.35)$$

and so, if the two involved random variables are independent from each other $\mathbb{E}[XY] = \mathbb{E}[X]\mathbb{E}[Y]$ and the covariance is equal to zero. Noticing it is properly the term that appears in the first mixed product between X_0 and V_0 , and they are clearly two independent quantities, we can draw the same conclusion. Instead, we can demonstrate that also the second and third mixed products are equal to zero considering the independence between involved variables and the stochastic

integral properties. For the second one, for example, it states:

$$\begin{aligned}
 & \mathbb{E} \left[(X_0 - \mathbb{E}[X_0]) \frac{1}{(\alpha - \beta)\sqrt{N}} \left(e^{\frac{(\alpha-\beta)t}{m}} \int_0^t e^{-\frac{(\alpha-\beta)s}{m}} dW_s - \int_0^t 1 dW_s \right) \right] = \\
 & = \mathbb{E}[(X_0 - \mathbb{E}[X_0])] \frac{1}{(\alpha - \beta)\sqrt{N}} \mathbb{E} \left[\left(\int_0^t e^{-\frac{(\alpha-\beta)s}{m}} dW_s - \int_0^t 1 dW_s \right) \right] = \\
 & = \frac{1}{(\alpha - \beta)\sqrt{N}} \mathbb{E}[(X_0 - \mathbb{E}[X_0])] \underbrace{\mathbb{E} \left[\left(\int_0^t e^{-\frac{(\alpha-\beta)s}{m}} dW_s \right) \right]}_{=0 \text{ for It\^o properties}} + \\
 & \quad - \frac{1}{(\alpha - \beta)\sqrt{N}} \mathbb{E}[(X_0 - \mathbb{E}[X_0])] \underbrace{\mathbb{E} \left[\left(\int_0^t 1 dW_s \right) \right]}_{=0 \text{ for It\^o properties}} = 0.
 \end{aligned}$$

The same result is obtained for the third mixed product between V_0 and the stochastic integrals difference. Then, in order to rewrite the variance of the swarm center of mass position, what remains is to rearrange the term $\mathbb{E}[(\clubsuit)^2]$, and so:

$$\begin{aligned}
 \mathbb{E}[(\clubsuit)^2] &= \frac{1}{(\alpha - \beta)\sqrt{N}} \mathbb{E} \left[\left(e^{\frac{(\alpha-\beta)t}{m}} \int_0^t e^{-\frac{(\alpha-\beta)s}{m}} dW_s - \int_0^t 1 dW_s \right)^2 \right] = \\
 &= \frac{1}{(\alpha - \beta)^2 N} \mathbb{E} \left[e^{\frac{2(\alpha-\beta)t}{m}} \left(\int_0^t e^{-\frac{(\alpha-\beta)s}{m}} dW_s \right)^2 + \left(\int_0^t 1 dW_s \right)^2 + \right. \\
 & \quad \left. - 2e^{\frac{(\alpha-\beta)t}{m}} \int_0^t e^{-\frac{(\alpha-\beta)s}{m}} dW_s \int_0^t 1 dW_s \right] = \\
 & \stackrel{(*)}{=} \frac{1}{(\alpha - \beta)^2 N} e^{\frac{2(\alpha-\beta)t}{m}} \int_0^t e^{-\frac{2(\alpha-\beta)s}{m}} ds + \frac{1}{(\alpha - \beta)^2 N} \int_0^t 1 dt + \\
 & \quad - \frac{2}{(\alpha - \beta)^2 N} e^{\frac{(\alpha-\beta)t}{m}} \underbrace{\mathbb{E} \left[\int_0^t e^{-\frac{(\alpha-\beta)s}{m}} dW_s \int_0^t 1 dW_s \right]}_{(*)}.
 \end{aligned}$$

At the passage (*) we made use of the *It\^o isometry*, and at this point we again exploit it, but in a generalized form:

$$\mathbb{E} \left[\int_0^t f(s) dW_s \int_0^t g(s) dW_s \right] = \int_0^t f(s)g(s) ds \quad (2.36)$$

and, consequently, we can rewrite the last term as follow

$$(*) = -\frac{2}{(\alpha - \beta)^2 N} e^{\frac{(\alpha-\beta)t}{m}} \int_0^t e^{-\frac{(\alpha-\beta)s}{m}} ds. \quad (2.37)$$

Now, collecting all these last results, we obtain:

$$\begin{aligned}
 \mathbb{E}[(\clubsuit)^2] &= -\frac{1}{(\alpha - \beta)^2 N} e^{\frac{2(\alpha - \beta)t}{m}} \frac{m}{2(\alpha - \beta)} \left[e^{-\frac{2(\alpha - \beta)t}{m}} - 1 \right] + \frac{1}{(\alpha - \beta)^2 N} t + \\
 &\quad + \frac{2}{(\alpha - \beta)^2 N} e^{\frac{(\alpha - \beta)t}{m}} \frac{m}{(\alpha - \beta)} \left[e^{-\frac{(\alpha - \beta)t}{m}} - 1 \right] = \\
 &= \frac{m}{2(\alpha - \beta)^3 N} \left[e^{\frac{2(\alpha - \beta)t}{m}} - 1 \right] + \frac{m}{(\alpha - \beta)^3 N} \left[1 - e^{\frac{(\alpha - \beta)t}{m}} \right] + \frac{1}{(\alpha - \beta)^2 N} t = \\
 &= \frac{m}{2(\alpha - \beta)^3 N} \left[e^{\frac{2(\alpha - \beta)t}{m}} - 2e^{\frac{(\alpha - \beta)t}{m}} + 1 \right] + \frac{1}{(\alpha - \beta)^2 N} t.
 \end{aligned} \tag{2.38}$$

Finally, we can write the expression for the variance of the swarm center of mass position, which was our goal:

$$\begin{aligned}
 \text{Var}(X) &= \text{Var}(X_0) + \frac{1}{(\alpha - \beta)^2 N} t + \\
 &\quad + \frac{m^2}{(\alpha - \beta)^2} \left[e^{\frac{(\alpha - \beta)t}{m}} - 1 \right]^2 \left(\text{Var}(V_0) + \frac{1}{2m(\alpha - \beta)N} \right).
 \end{aligned} \tag{2.39}$$

It's interesting to notice that at $t = 0$, $\text{Var}(X) = \text{Var}(X_0)$, and it shows how at the initial moment the variance depends only on the variance of the initial swarm configuration.

Considering equation (2.39), we can now analyze different regimes of the system depending on parameters α and β . The procedure is similar to the one followed in the previous section, but in this case we can interpret results taking into account the time dependence of the center of mass position variance (which is related to the mean squared displacement). The case $\alpha > \beta$ determines a regime of extremely rapid diffusion, in which the variance shows an exponential growth in time. Rearranging equation (2.39), we obtain

$$\begin{aligned}
 \text{Var}(X) &= \text{Var}(X_0) + \frac{1}{(\alpha - \beta)^2 N} t + \\
 &\quad + \frac{m^2}{(\alpha - \beta)^2} e^{\frac{2(\alpha - \beta)t}{m}} \left[e^{-\frac{(\alpha - \beta)t}{m}} - 1 \right]^2 \left(\text{Var}(V_0) + \frac{1}{2m(\alpha - \beta)N} \right).
 \end{aligned} \tag{2.40}$$

In the long time limit ($t \gg m/(\alpha - \beta)$) the term within square brackets with negative exponent vanishes, and we clearly observe an exponential trend (contributions

of the initial condition to the position variance and the linearly growing term are overcome):

$$\text{Var}(X) \sim \mathcal{C} e^{\frac{2(\alpha-\beta)}{m}t}, \quad (2.41)$$

where \mathcal{C} is a constant depending on initial variance and model parameters. We can notice that also the expected value of the swarm center of mass position exhibits an exponential growth. Here it's interesting to emphasize that, even if the initial variance of the swarm velocity were equal to zero (it would mean that we are considering a Dirac delta distribution for the initial velocities, for example assuming that all particles has zero initial speed), the terms generated by stochastic noise would lead to exponential trend. So, we can state that the finiteness of the swarm, since it's composed by a finite number of units, determines an increasing uncertainty over time on the swarm center of mass position (and velocity, as shown in the previous section). In the $\alpha < \beta$ case, again from equation (2.39) and from (2.33), we get

$$\text{Var}(X) = K + \frac{1}{(\alpha - \beta)^2 N} t, \quad (2.42)$$

and

$$\mathbb{E}[X] = \mathbb{E}[X_0] + \frac{m}{(\beta - \alpha)} \mathbb{E}[V_0], \quad (2.43)$$

where K is a constant depending on initial conditions and on model parameters. We can observe that, even if the expected value reaches a constant magnitude, the variance continues to grow linearly in time. This allows us to recognize a *normal diffusion* regime: the center of mass of the swarm wanders around the mean position because of the stochastic fluctuations affecting the microscopic dynamics of each particle. I want also to point out that the linear dependence on time is predicted by the *Ornstein-Uhlenbeck* model for large times. This is clear if we rewrite equation (2.13) substituting $(\beta - \alpha) > 0$ with a new constant γ . So, the equation becomes

$$mdV = -\gamma V dt + \frac{1}{\sqrt{N}} dW_t, \quad (2.44)$$

and it is formally equivalent to (A.1) treated in the Appendix. Moreover, writing the linear Taylor expansion of exponential term in equation (2.39), $e^{-\frac{\gamma}{m}t} \approx 1 - \frac{\gamma}{m}t$, we obtain:

$$\text{Var}(X) \approx \text{Var}(X_0) + \frac{1}{\gamma^2 N} t + \left(\text{Var}(V_0) - \frac{1}{2m\gamma N} \right) t^2. \quad (2.45)$$

We can notice that the variance of the position scales quadratically with time, for small times ($t \ll m/(\alpha - \beta)$), as expected.

Finally, in order to analyze the case $\alpha = \beta$, we have to manipulate equation (2.28),

because in the following ones the difference between the two coefficients appears as denominator. Imposing the equality condition, the equation takes the form

$$V = V_0 + \frac{1}{m\sqrt{N}} \int_0^t dW_s, \quad (2.46)$$

and integrating it, we get the following position equation:

$$X = X_0 + V_0 t + \frac{1}{m\sqrt{N}} \underbrace{\int_0^t \int_0^\tau dW_s d\tau}_{(\dagger)}, \quad (2.47)$$

in which there is a double integral with respect to time and Wiener process. Here we exploit again integration by parts, and, considering

$$\begin{aligned} u &= \int_0^t dW_s & v &= \int_0^t d\tau \\ du &= dW_t & dv &= d\tau, \end{aligned}$$

we obtain the following expression:

$$(\dagger) = \int_0^t dW_s \int_0^\tau d\tau - \int_0^t \tau dW_\tau = t \int_0^t dW_s - \int_0^t \tau dW_\tau. \quad (2.48)$$

At this point we evaluate the expected value of the swarm center of mass position,

$$\mathbb{E}[X] = \mathbb{E}[X_0] + \mathbb{E}[V_0]t + \mathbb{E}\left[t \int_0^t dW_s - \int_0^t \tau dW_\tau\right] = \mathbb{E}[X_0] + \mathbb{E}[V_0]t, \quad (2.49)$$

in which the last step is again justified by *Itô integral* properties. Then we can calculate the variance

$$\text{Var}(X) = \mathbb{E}\left[(X_0 - \mathbb{E}[X_0])^2 + (V_0 - \mathbb{E}[V_0])^2 t^2 + \frac{1}{m^2 N} \left(t \int_0^t dW_s - \int_0^t \tau dW_\tau\right)^2\right], \quad (2.50)$$

in which again the double products are equal to zero, as demonstrated previously. Now, focusing on the last term, we can rewrite it as:

$$\begin{aligned} \frac{1}{m^2 N} \mathbb{E}\left[t^2 \left(\int_0^t dW_s\right)^2 + \left(\int_0^t \tau dW_\tau\right)^2 - 2t \int_0^t dW_s \int_0^\tau \tau dW_\tau\right] &= \\ &= \frac{1}{m^2 N} \left[t^3 + \frac{t^3}{3} - 2t \frac{t^2}{2}\right] = \frac{1}{m^2 N} \frac{t^3}{3}, \end{aligned} \quad (2.51)$$

and in this last equality we made use once again of the *Itô isometry*. Collecting all these results we obtain a clearer expression for the variance

$$\text{Var}(X) = \text{Var}(X_0) + \text{Var}(V_0)t^2 + \frac{1}{m^2N} \frac{t^3}{3}. \quad (2.52)$$

Now we can easily observe how, in this last case, the expected value of the swarm center of mass position grows linearly in time, while the variance has a cubic growth. Considering the form of the variance evolution function, we can recognize a *super-diffusion* regime, which takes place when $\langle r^2 \rangle \propto t^\theta$, with $\theta > 1$, and so when the *mean squared displacement* depends on time more than linearly. This fact can be explained noticing that, in this last case, the alignment effect balances the damping force, which usually in *Brownian motion* has the role of a restoration term, which tends to bring back the particles towards the average position.

The fundamental and far-reaching result, that emerged from the statistical analysis of the current mathematical model, is that the *finiteness* of natural swarm, be they animal groups or human crowds, determines an increasing uncertainty both on position and velocity of the swarm center of mass over time. Even if we consider really numerous ensemble, such as insect swarms, after a certain time interval, the stochastic fluctuations contribution becomes relevant, and it can not be neglected. And this observations holds for each of the three parameters regime. Moreover, we can notice that the noise term is inversely proportional to the number of particles N , and so a massive swarm results to be more stable. It means that a numerous ensemble tends to maintain its position and velocity, if it is actively moving, better than a swarm composed by a small number of individuals. We can find lots of natural examples in which large groups take advantage from maintaining constant direction of motion. We can think about birds migration, insect swarms movement towards a target site for nesting or for searching new resources, or about cell population collective motion. We can also interpret the present result in light of evolution theory. In fact, we can notice that, since a large number of individuals hides or mitigate the effect of noise fluctuations on collective dynamics, the need to optimize movement has favoured the aggregation in large groups.

Chapter 3

Numerical simulations

In order to evaluate the goodness of the model predictions, in this section I report numerical outputs from several simulations performed with different conditions. In the first part I show how setting $l_c = 1000$ guarantees that equation (2.12) adequately approximates the swarm center of mass dynamics, even in the case without noise. It is reasonable since we considered a swarm composed by a large number of particles. With this in mind, I analysed the behaviour of the current model in the three regimes we identified on the basis of ratios between the alignment and friction parameters. Each of them characterizes the evolution over time of the swarm dynamics, and I describe it in terms of velocity and position referred to the center of mass and to a single generic particle we named "Alice". Then I studied the difference in numerical outputs considering different values of the alignment characteristic length l_c , that, as already pointed out, describes how much the average process deviates from an unweighted average. Moreover, the simulations of the first part provide a clear representation of the spatial patterns generated by the collective dynamics. In each section a brief discussion follows the presentation of results, in order to underline interesting aspects or to propose an adequate interpretation of them.

In the second part I propose numerical simulations output to verify results from the 1D statistical analysis of the swarm center of mass dynamics performed in the previous section. Basically the first part allows to directly compare the statistical analysis results with numerical outputs from the simulation of the swarm center of mass equation rather than considering the microscopic dynamics of all the particles. This choice is justified by the high computational cost that characterizes this second way, since it is far beyond the capabilities of an average computer. All the simulations are carried out using the software MATLAB, since our problem is particular suitable to a matrix formalization. In fact, the vector particle dynamics equations are solved as two independent scalar equations in each spatial variable.

3.1 Methods

All the simulation in the first part has been performed initializing a swarm composed by $N = 1000$ particles, in order to obtain a reasonable averaged stochastic fluctuations. In fact, if we consider only a bunch of particles, the influence of the noise term would be too strong to compare numerical and deterministic analytical results. Moreover, as introduced in the previous section, all particles have a similar size, and so we model this condition setting unitary mass for each of them.

The initial position and velocity of each particle are considered as random variables. Here in particular we chose a *standard normal distribution* as probability density function (so, a Gaussian with zero mean and unitary variance). Consequently, we obtain the initial spatial configuration of the swarm extracting the x and y coordinates for each individual, and the same holds also for the velocity components. Figure (3.1) graphically represents the positioning process which gives place to the

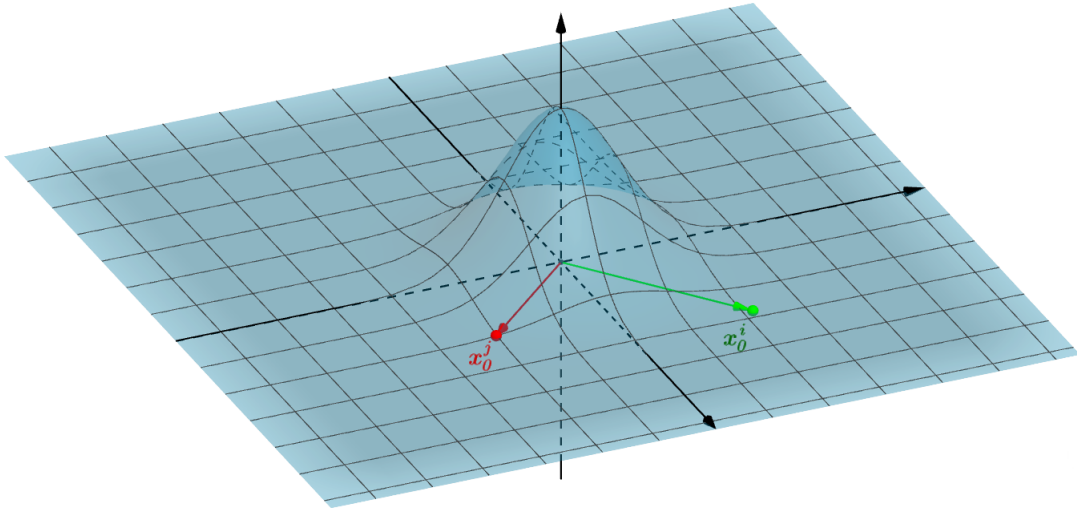


Figure 3.1: Graphical representation of the random initial placement of two particles.

initial spatial configuration of the swarm. The value extracted from the normal distribution, with a certain probability, is then multiplied by a factor of 2.5, in order to obtain an initial configuration scattered on a wider area, but with most of particles gathered in the middle. The other parameters of the simulations, which remain unchanged in all cases, are collected in Table (3.1). Here I want to point out that all the parameters are dimensionless, and they units of measurement depend on the specific case study. For each regime I performed two different simulations.

Simulation parameters	
Number of time steps	$1.5 \cdot 10^4$
Time steps - dt	10^{-3}
Number of particles - N	1000
Particle mass - m	1
Positioning factor	2.5
Attraction characteristic strength - C_a	0.5
Attraction characteristic length - l_a	2
Repulsion characteristic strength - C_r	1
Repulsion characteristic length - l_r	0.5
Alignment characteristic length - l_c	$10 - 10^3$

Table 3.1: This table collects the parameters which remain unchanged for all the simulations of the first part.

In the first one we set $l_c = 10$, so the alignment characteristic length is such that the alignment process is more affected by closest neighbours velocities. Indeed, in order to quantify this effect, we can observe that in the current setting conditions the limit diameter of the swarm is approximately equal to 4 units of length. So, if we consider the i -th particle, the factor which multiplies the velocity of a neighbour placed on the other side of the swarm is equal to $e^{-(4/10)} \approx 2/3$. Then, we can notice that a really close individual exerts an alignment effect on the dynamics of

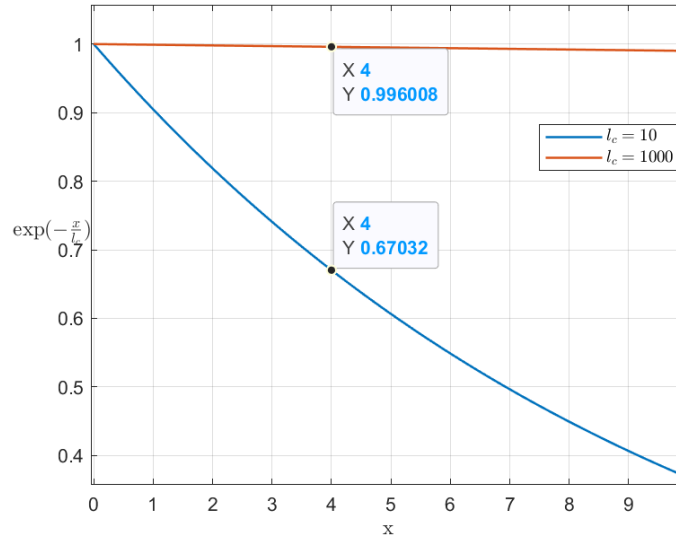


Figure 3.2: Difference between $l_c = 10$ and $l_c = 10^3$ cases. The plot shows the alignment factors as distance functions in the weighted average process.

the i -th particle about 1.5 times greater than the one exerted by another agent placed on the edge of the swarm. In the second case, instead, we consider $l_c = 1000$, and consequently the alignment process tends to an unweighted average process. This second case represents a stronger physical assumption, but it provides output in better agreement with the analytical model we derived for the swarm center of mass. Finally, we solved the stochastic differential equation defining the swarm dynamics (2.1) through the *Euler-Maruyama* method. It is the analogous of *Euler method* for stochastic differential equations. In this method the *Wiener process* is approximated as a Markov chain, and such a discretization is used to compute the stochastic integral (more information about the *Euler-Maruyama* method in the Appendix).

3.2 Comparison between microscopic dynamics and deterministic results

3.2.1 The accelerated regime

As I already pointed out, we identified three different regimes for the current model, and they depend on the balance between the alignment contribution and the friction term, which appear in the dynamics equation. In this section I firstly introduce the regime characterized by the condition $\alpha > \beta$, that describes the situation in which the alignment effect is stronger than the damping. Consequently the swarm shows collective net motion, and it is the only case in which we can observe an increasing center of mass velocity over time.

Here I compare numerical results with the analytical function derived from the deterministic version of equation (2.12). Indeed, neglecting the noise term, since we can assume that it vanishes for an increasing number of individuals (at least up to a reasonable time), and integrating it, we obtain

$$V(t) = V_0 e^{\frac{(\alpha-\beta)}{m}t}, \quad (3.1)$$

where it holds for each scalar component of the vector equation (the equation for the velocity modulus simply has a factor 2 multiplying the exponent, and the initial modulus as initial value). Integrating again, we get the equation for the position of the center of mass

$$X(t) = X_0 + \frac{m}{(\alpha - \beta)} V_0 \left[e^{\frac{(\alpha-\beta)}{m}t} - 1 \right]. \quad (3.2)$$

I want to emphasize that we neglect the noise term only in deriving the analytical equations for velocity and position of the swarm center of mass, and that we consider these analytical functions as reference mean results. In this case I set the

alignment strength $\alpha = 1$ and the friction coefficient $\beta = 0.5$. Firstly I want to present numerical outputs from simulations carried out with $l_c = 10$.

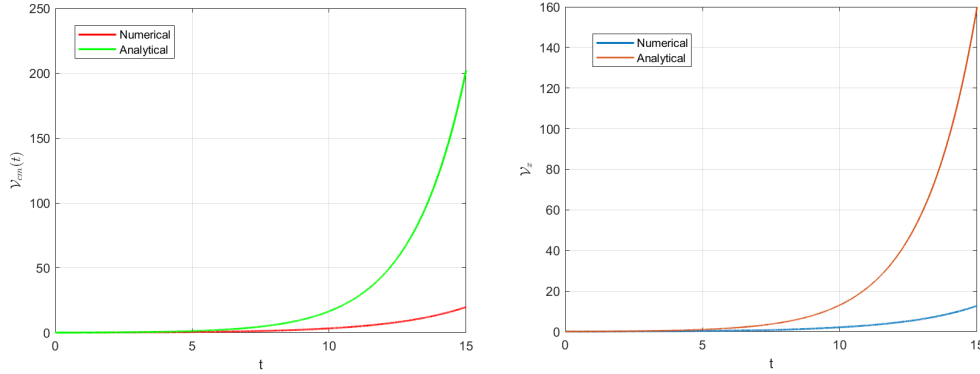
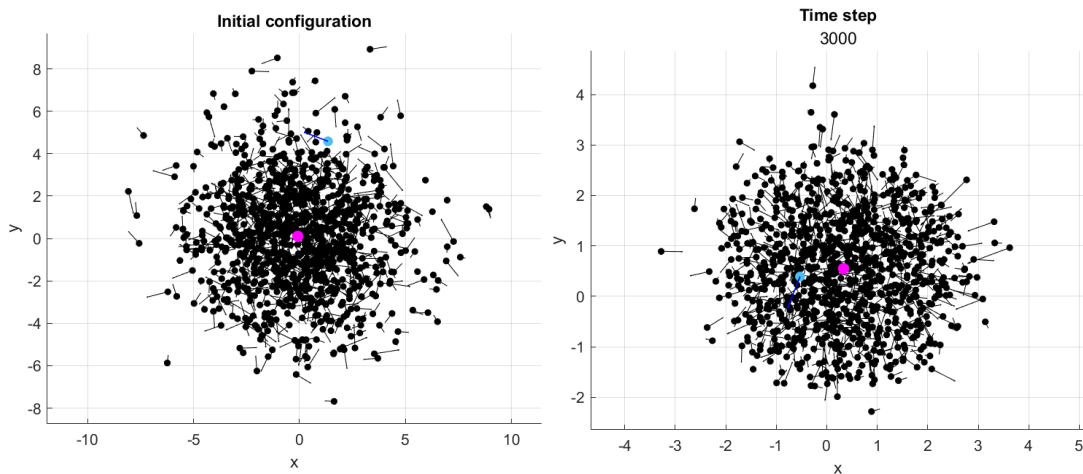


Figure 3.3: Center of mass modulus and x-velocity over time.

Figure (3.3) shows the center of mass modulus and x-velocity components trends over time. The first thing that catches your eye is that numerical result grows slower than the analytical prediction. This difference is due to the lower value of l_c , which determines a slower alignment process, since each particle perceives majorly the closest neighbours than the others. Nevertheless the velocity modulus still shows an exponential trend, and this also holds true for the two scalar components separately. Even the position (Figure (3.5), left picture), as described by equation (3.2), presents the same trend. Figure (3.4) collects snapshots at different time, and they represent the emergence of collective motion during the numerical simulation. Indeed, we can notice that up to 6000 time steps the swarm is still rearranging, while the alignment process is well visible in the next snapshot. From this point, the swarm continues to maintain the same direction (as shown in Figure (3.5), right



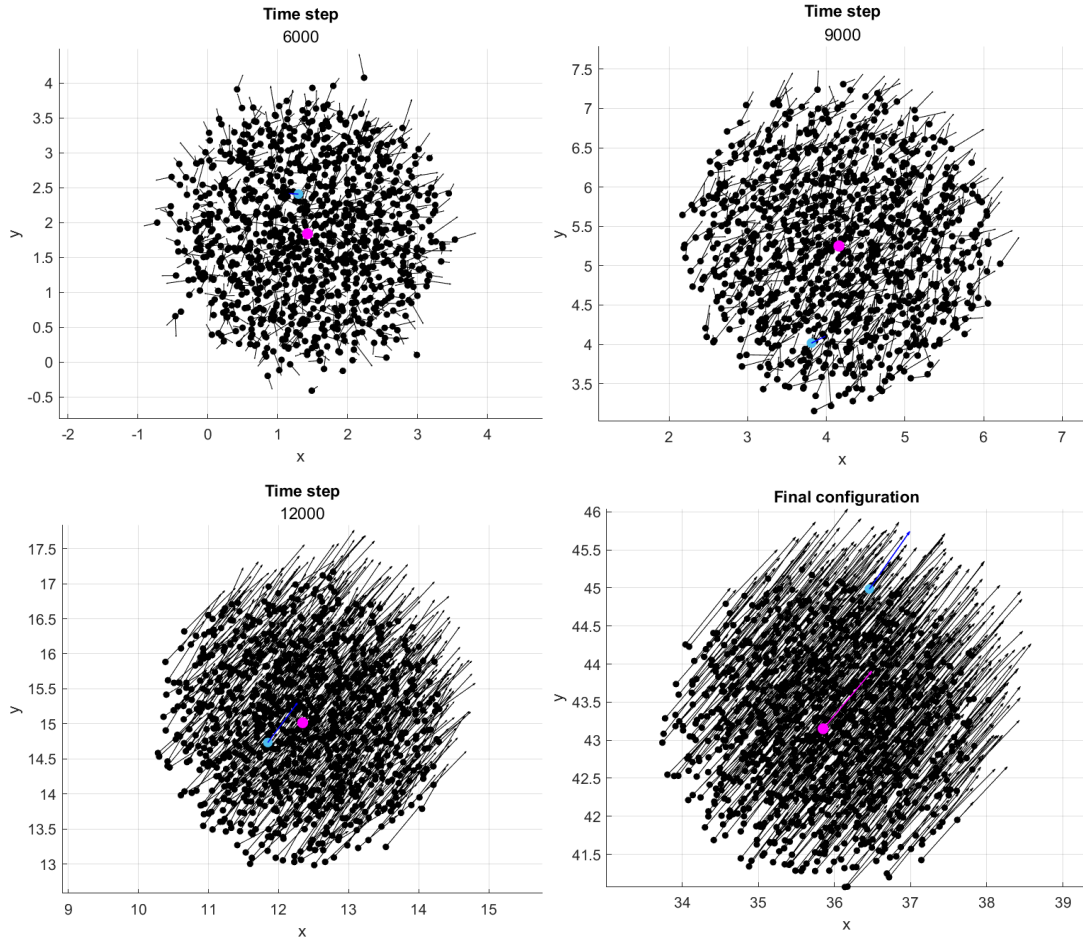


Figure 3.4: Series of images representing the evolution of the swarm configuration over time. The time step of each snapshot is reported. The pink dot represents the center of mass, while the light blue one is the "Alice" particle.

picture), accelerating exponentially over time. In order to point out the difference between the center of mass and the the single particle behaviour, we numerically computed also position and velocity evolution for the "Alice" particle. As shown in Figure (3.6), "Alice" too follows an exponential-like displacement trend, while the x-velocity component is subjected to stronger fluctuations, due to the effect of the stochastic noise, which in this case is not averaged on the entire swarm.

The really fascinating phenomenon is the emergence of collective behaviour from an initial random configuration. Indeed, in this case, particles spontaneously align and start to migrate with increasing velocity. The direction of motion depends only on the initial conditions (as defined in equation (3.1)), and so, if we consider the two scalar spatial components, we can notice that it finally depends on the two values

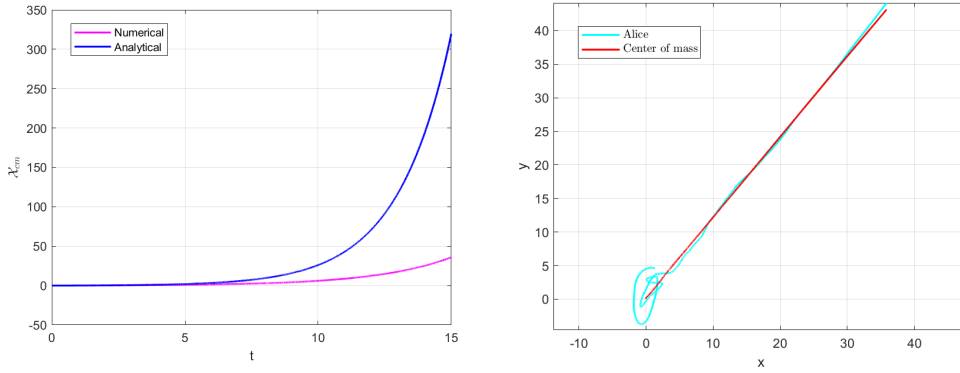


Figure 3.5: Center of mass x-displacement (left), and trajectories of the center of mass and of the "Alice" particle.

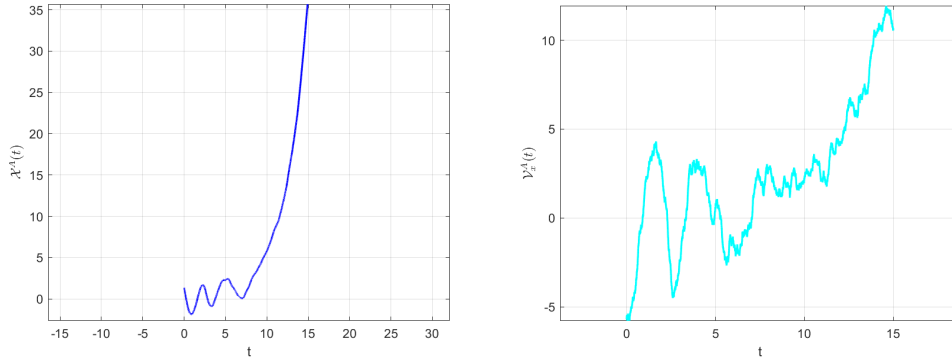


Figure 3.6: Numerical output for "Alice" position and x-velocity during the simulation.

extracted as realizations of normally distributed random variables. Mathematically speaking, the appearance of self-organization depends on the coupling between particle microscopic dynamics performed by the alignment term. I find also very interesting that numerical simulations show how, even if we do not consider a perfect average process (as done in the Vicsek model, and which could results in a too strict physical assumption), the collective dynamics still takes place and develops over time.

Now I want to report numerical results also about the $l_c = 1000$ case, since it provides the occasion to highlight other important aspects of the current model. Observing Figure (3.7), we can observe that numerical outputs about the swarm center of mass velocity well match the analytical results, better than in the previous case. The residual noise is recognizable in the zoomed area. Figure (3.8), left picture, compared with the configuration at the same time step in the $l_c = 10$ case, reveals a stronger alignment between swarm agents. This effect involves both the

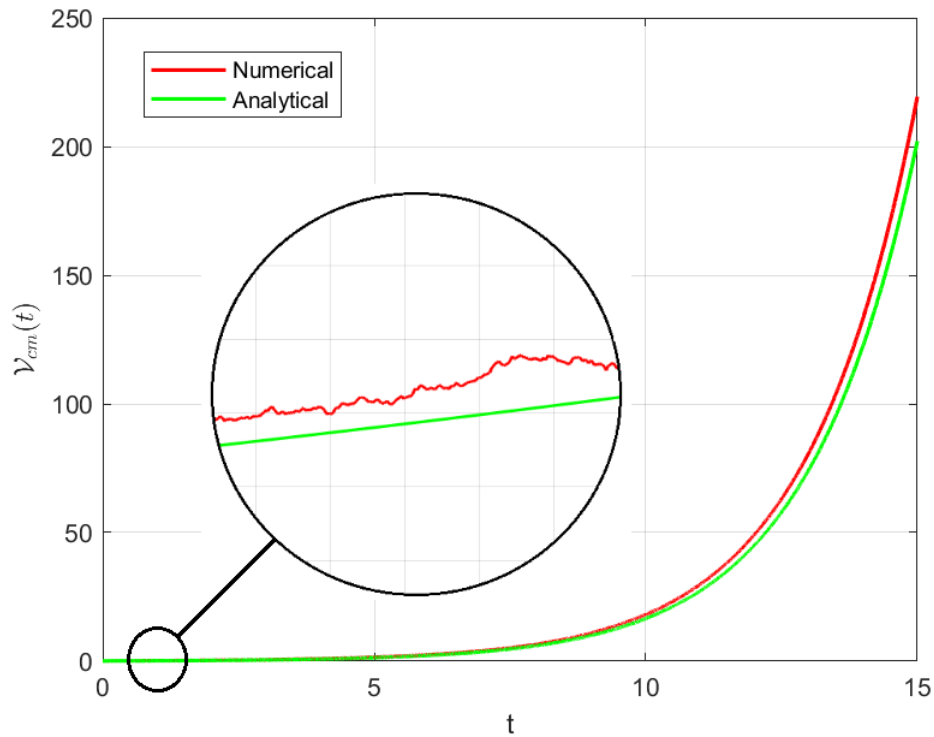


Figure 3.7: Swarm center of mass velocity during a simulation. Comparison between analytical and numerical results in the case $l_c = 1000$.

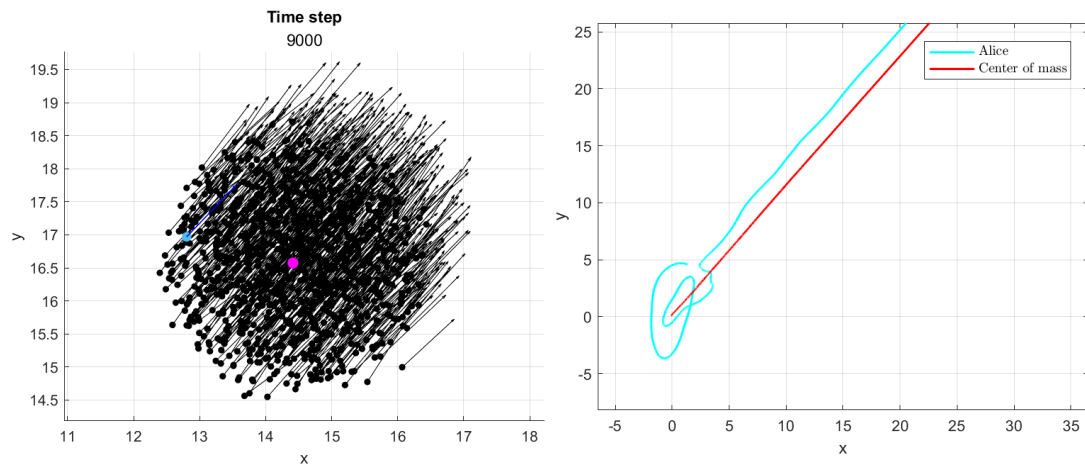


Figure 3.8: Alignment of the swarm after 9000 time steps. Initial evolution of center of mass and "Alice" trajectories.

modulus and the direction of particles velocity. In fact, they move faster and also in a more coherent way, and it is because the unweighted average procedure provides

a clearer alignment stimulus. The right picture represents the initial evolution of the "Alice" particle and center of mass trajectories. We can observe that after a brief rearrangement, "Alice" starts to move in parallel with the center of mass keeping a constant distance from it.

Finally, I want to emphasize that all those overdamped models (cited in the introduction), which involve a similar alignment mechanism, and that give net persistent motion as a result, automatically lay in this parameters regime.

3.2.2 The wandering center of mass regime

In this section I present numerical results about the case $\alpha < \beta$. In this condition the friction effect is stronger than the alignment one.

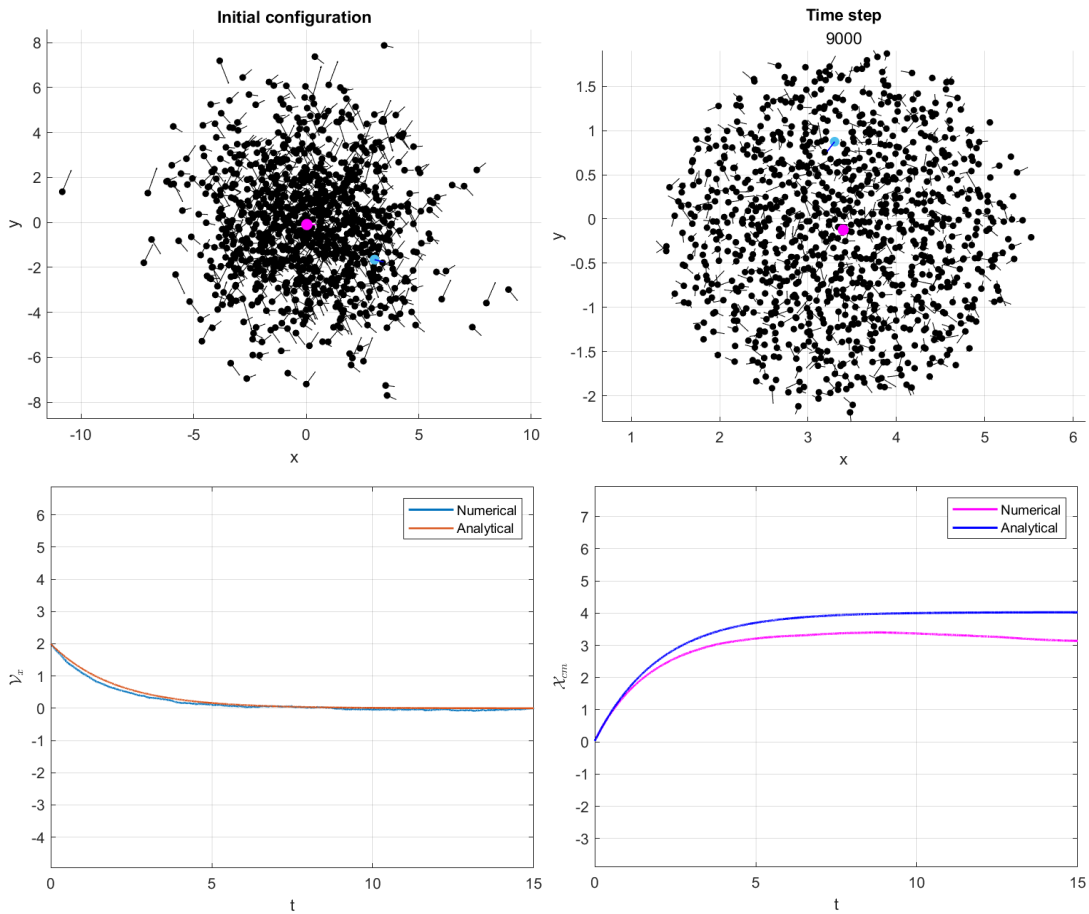


Figure 3.9: The first two pictures represent the swarm configuration at the beginning and after 9000 time steps. The latter concern evolution of the x component of center of mass velocity and position over time.

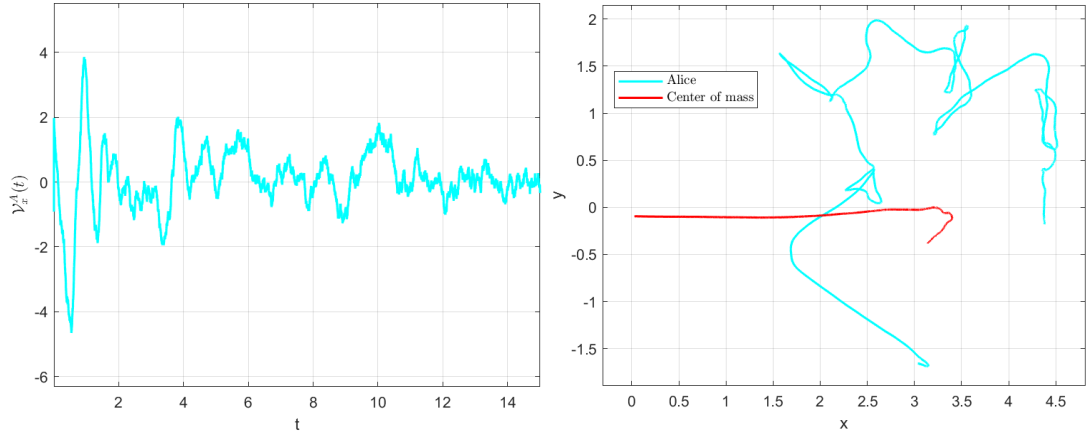


Figure 3.10: "Alice" x-velocity and trajectories of center of mass and "Alice" particle.

In particular I set $\alpha = 0.5$ and $\beta = 1$, and all the other parameters have the same values of the previous simulation. Since we expected a damped dynamics, which leads to zero mean swarm velocity, I set an initial average x-velocity equal to 2, in order to observe the evolution of the collective dynamics. Otherwise the swarm simply maintains its initial mean position, while the particles continue to wonder around the center of mass. Now we start considering the $l_c = 10$ case, as I have done before. We can observe from the first two pictures in Figure (3.9) that, even if in the initial configuration a positive x-velocity component is recognizable, after 9000 time steps it has been lost because of the friction term action. The last two pictures

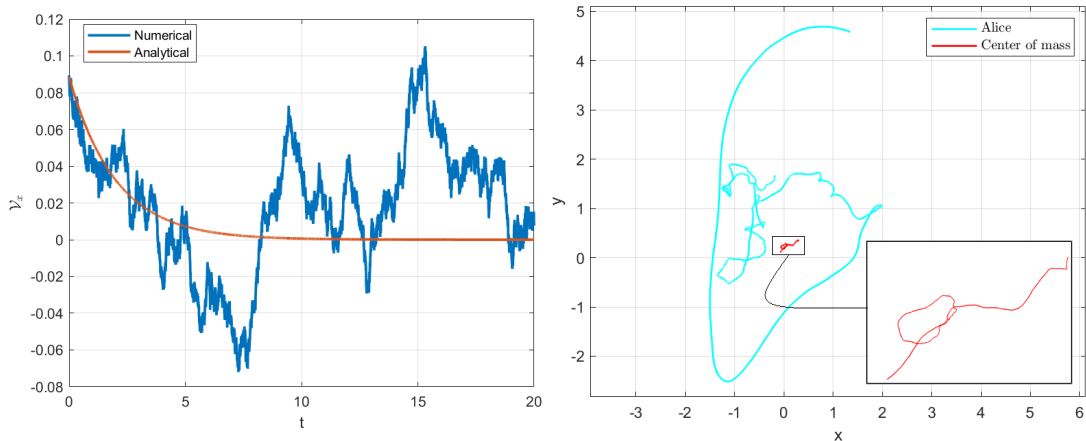


Figure 3.11: Center of mass velocity and trajectories in case of zero initial mean velocity.

show the evolution of the x component of velocity and position of the center of mass over time. Velocity rapidly decreases towards zero, while the displacement reaches a constant value depending on initial conditions, as derived in the previous chapter. I considered here only the x component, since I set non zero center of mass x -velocity as initial condition, but the dynamics of the velocity modulus is analogous. Figure (3.10), left picture, represents "Alice" x -velocity over time. We can observe that after the initial transient, the velocity of the particle continues to fluctuate around the mean zero value, as a results of the stochastic noise. The right picture, instead, shows the "Alice" and the center of mass trajectories. After an initial displacement, the center of mass stops and begins to wander around, while the "Alice" particle continues to move around it. Here I want to point out that,

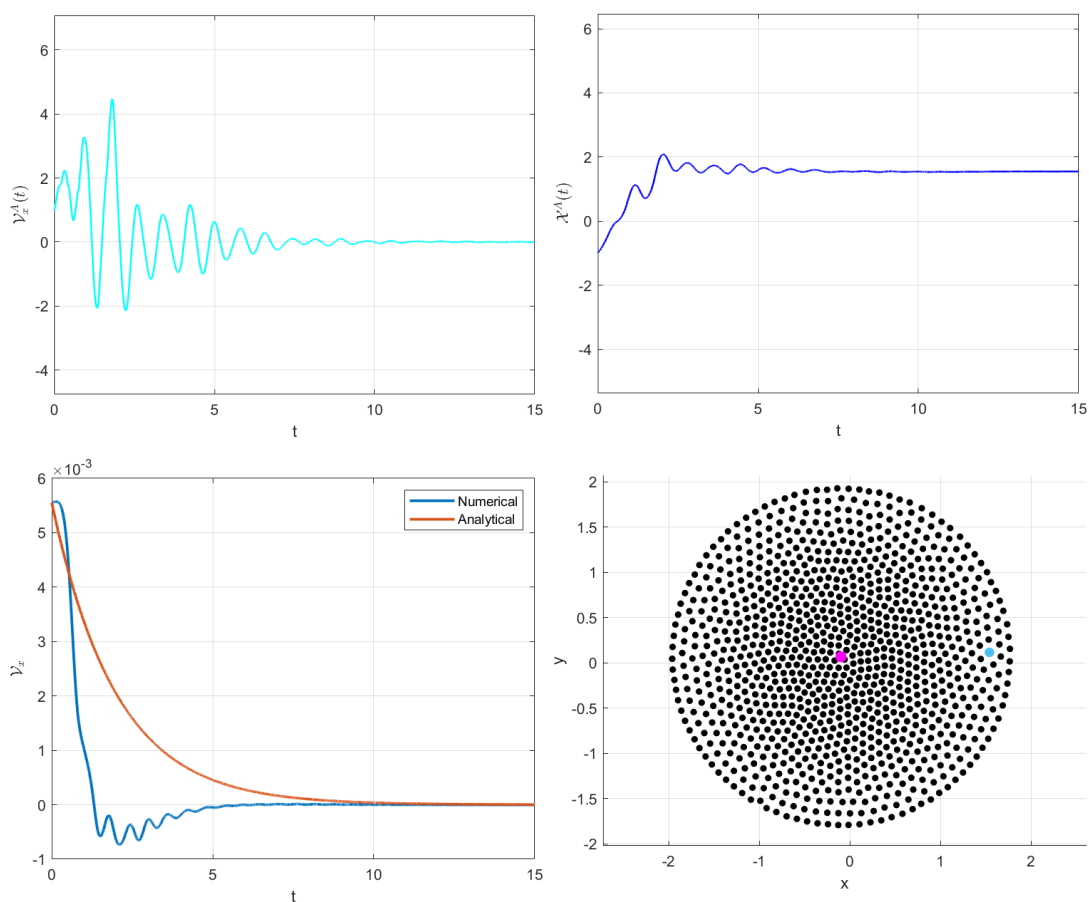


Figure 3.12: These pictures refer to the case without noise. The first two represent "Alice" particle velocity and displacement, while the latter show center of mass x-velocity and swarm final configuration.

once the swarm center of mass velocity reaches the mean zero value, its wandering

movement can be described as the result of a *Ornstein–Uhlenbeck process*. We showed this mathematical result in chapter 2, in which we derived the position expected value and variance. It's interesting that these two quantities show the expected behaviour for small times and also in the long time limit.

I want also to comment some results about the simulation with zero initial mean velocity. In this case the transient is very short and the center of mass rapidly reaches near zero velocity, as shown in the left picture of Figure (3.11). As a consequence it starts to wander around its initial position without performing translational movement, as represented in the right snapshot. I also analysed the case without noise, in order to observe the model response. Numerical results are reported in Figure (3.12). The "Alice" particle, which represents a generic particle of the system, reaches zero x-velocity and a constant displacement, without oscillations after the initial rearrangement, as shown in the first two images. The latters represent the x-velocity of the center of mass, which also reaches the zero value, and the final configuration of the swarm. Since there is no noise, particles don't wander around the mean position, and the crystalline pattern appears. Finally,

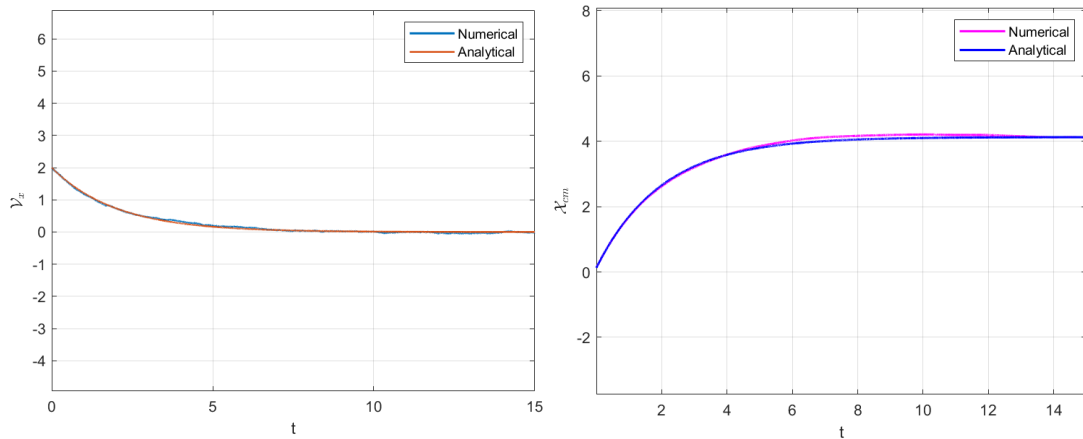


Figure 3.13: Center of mass velocity and displacement evolution during the simulation. Again only the x-component is considered.

in Figure (3.13) I report plots about center of mass velocity and displacement in the case $l_c = 1000$, with initial positive mean x-velocity. With this setting, numerical output again are in better agreement with the analytical result, especially in case of displacement results. It is because the assumption of large alignment characteristic length is better respected in this case. Moreover, the collective behaviour of the system is qualitatively similar to the case $l_c = 10$, and there are not differences in the dynamics of the system.

3.2.3 The invariant regime

The last parameters regime I analysed corresponds to a balance between the alignment contribution and the damping effect exerted by the friction term. This balance refers to the center of mass equation (3.1). Mathematically we have $\alpha = \beta$. Also in this case, since we expected the maintenance of the initial condition throughout the entire simulation, I set initial x-velocity equal to 2 (dimensionless unit of measurement). Considering the two parameters, I set $\alpha = \beta = 1$, while the rest of the simulation setting remained unchanged. Figure (3.14) collects snapshots of the swarm configuration evolution over time in the case $l_c = 10$. We can identify a positive x-velocity component in the first two picture, and it's clearly still present at 6000 time step. However, in the final configuration a collective net movement is not anymore recognizable, because of the balancing between alignment term and damping effect. Moreover, we can notice that the weighted average procedure

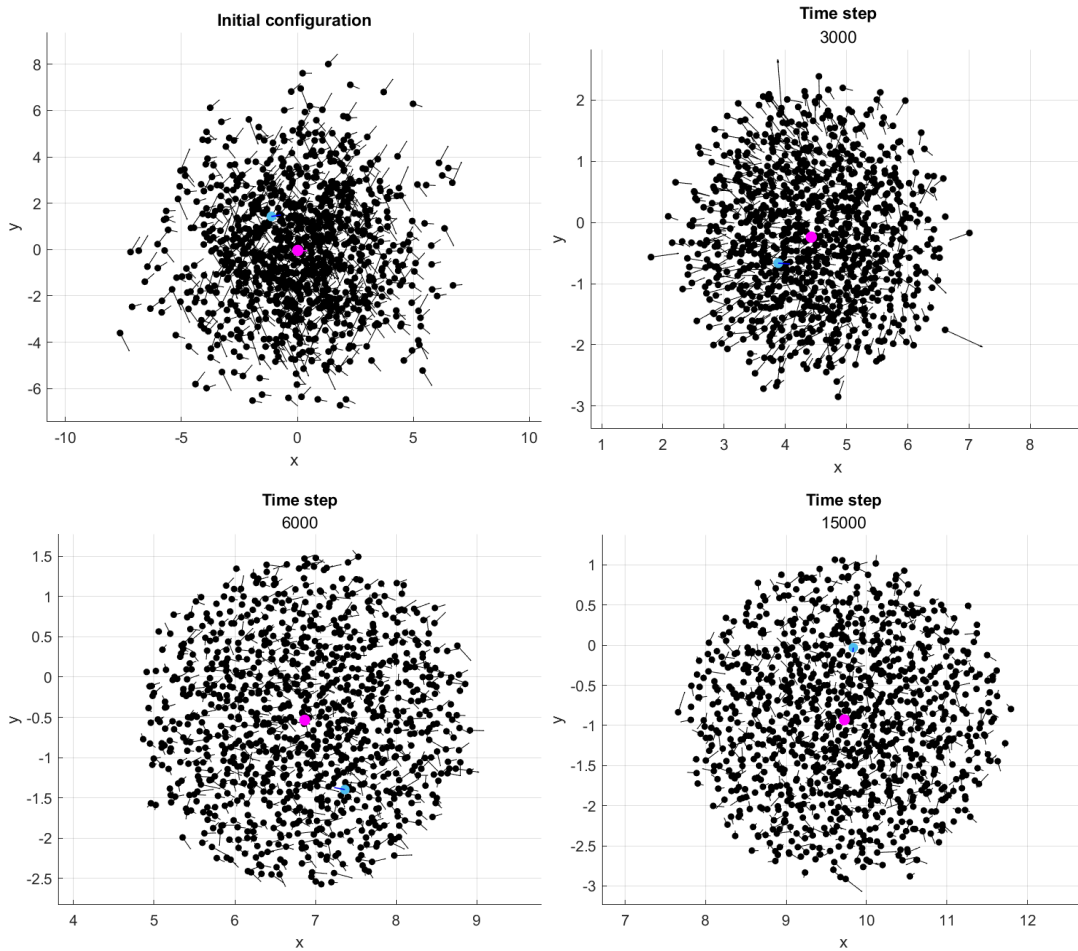


Figure 3.14: Evolution over time of the swarm configuration.

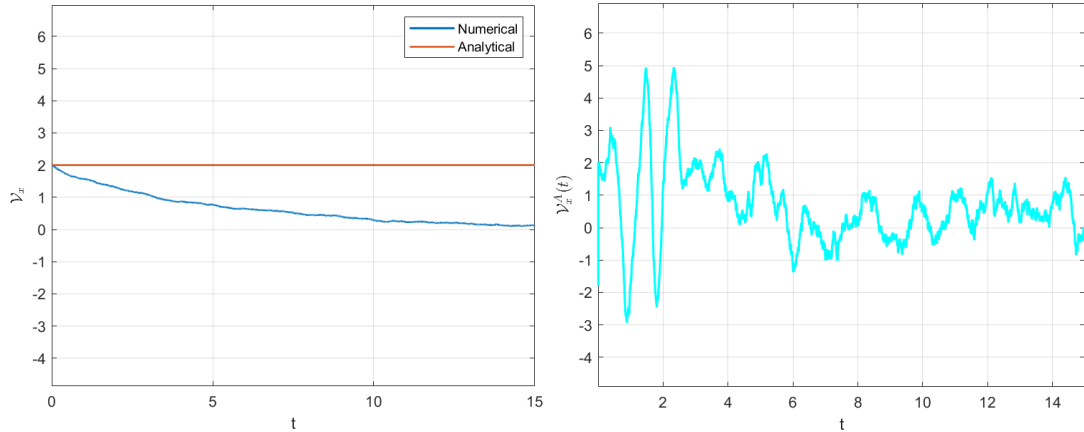


Figure 3.15: Center of mass and "Alice" particle x-velocity during a typical simulation with $l_c = 10$.

which accounts for the alignment contribution, in the case $l_c = 10$, is not sufficient to guarantee the internal cohesion of the swarm. This results in a progressive loss of efficiency in terms of translational collective movement. Left picture of Figure (3.15) compares analytical and numerical trends of the x-velocity of the swarm center of mass. We can notice a pronounced difference between them, since the numerical trend is approaching zero value with time. Instead, the right picture represents the evolution of "Alice" x-velocity. We can observe how, also in this case, the mean value of the stochastic process is moving towards zero. It is because, even if the swarm has initial positive x-velocity, at the end of the simulation it almost stops. Consequently, particles begin to wander around prone to the stochastic

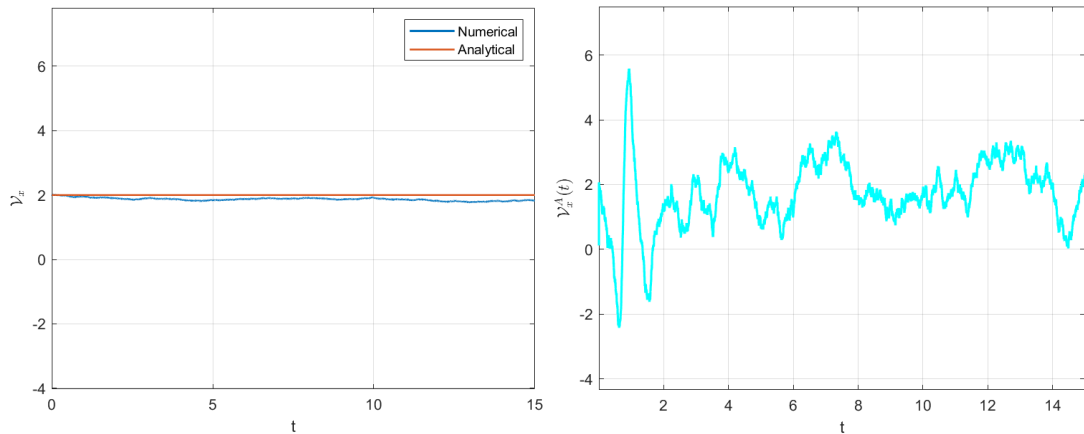


Figure 3.16: Center of mass and "Alice" x-velocity evolution over time ($l_c = 1000$).

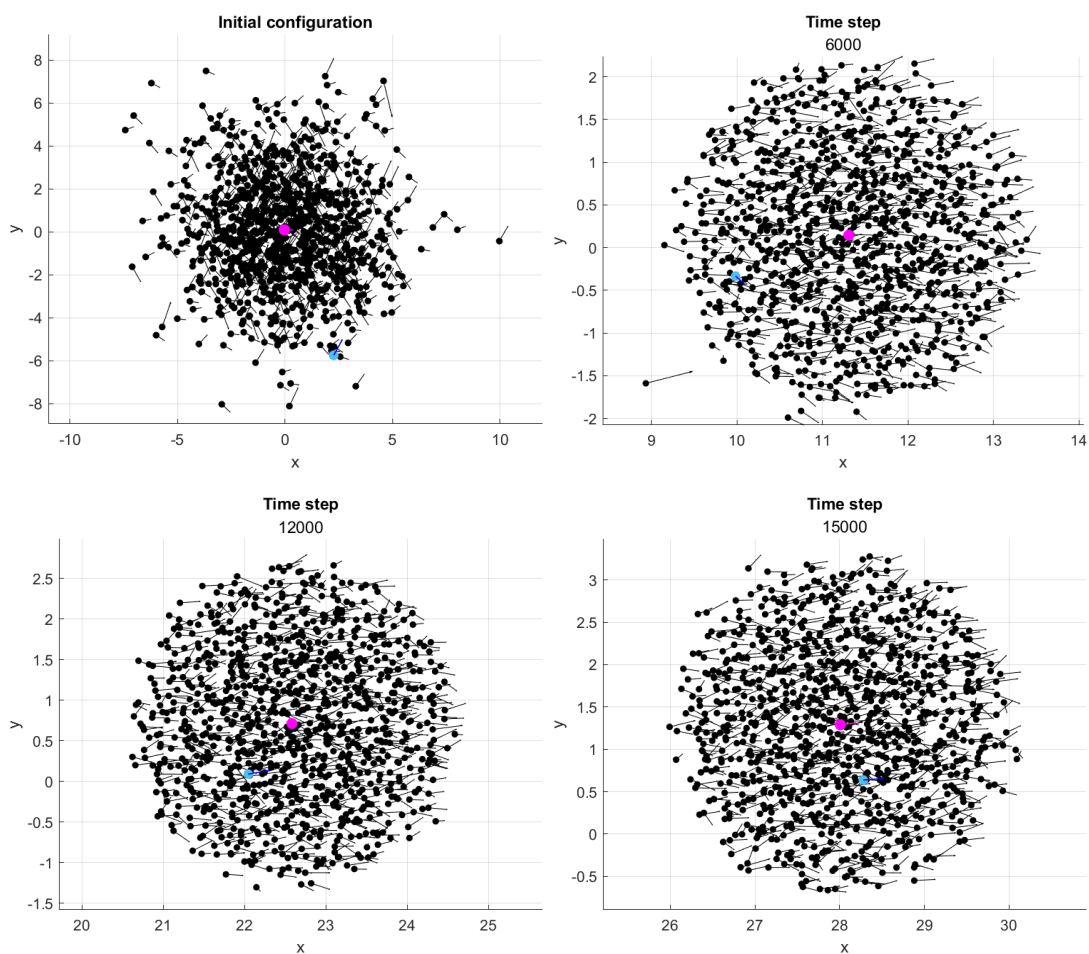


Figure 3.17: Snapshots of the spatial configuration of the swarm taken at different time steps ($l_c = 1000$).

noise fluctuations. Moreover, since the velocity of the swarm decreases during the simulation, the center of mass displacement is a non-linear function of time with decreasing slope and it reaches a constant asymptotic value (see Figure (3.18), right picture). Figure (3.16) represents the same quantities, but in the case of $l_c = 1000$. The difference between the two cases is clearly visible. Now, numerical outputs well approximate the analytical prediction, and the center of mass velocity maintains an almost constant trend. Obviously it continues to be subjected to small noise fluctuations, as represented in the left picture. The right picture in Figure (3.16) shows the "Alice" x-velocity during the simulation. If we compare it with its analogous in Figure (3.15), we now can notice that the fluctuations take place around a non-zero mean value, which is the initial x-velocity value of the swarm center of mass.

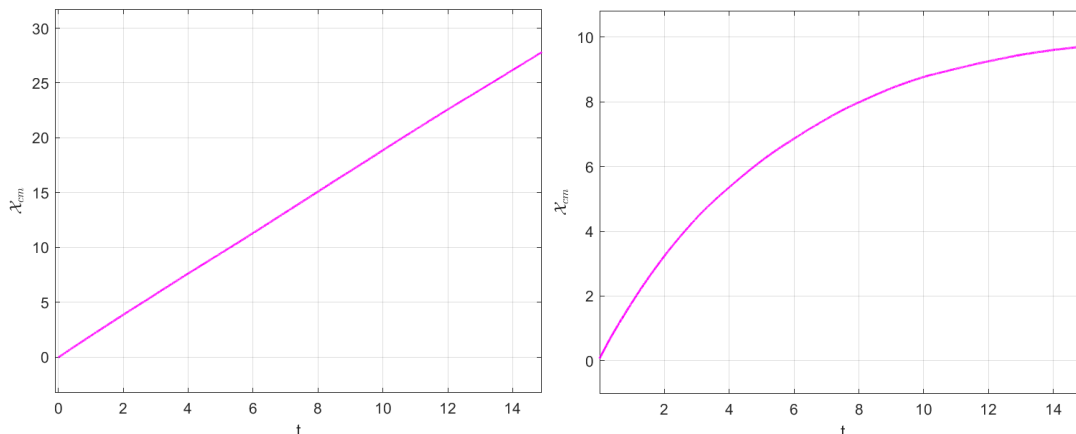


Figure 3.18: Comparison between x-displacement of the center of mass for $l_c = 1000$ and $l_c = 10$.

Figure (3.18) represents the center of mass x-displacement. Since the velocity is almost constant during the simulation, the displacement now grows linearly over time, how we can observe in the left picture. I also report some snapshots of the evolution of the spatial configuration of the swarm over time in Figure (3.17). The main difference with the previous case is that we can observe collective net motion also in the last time step. It is a consequence of the fact that the center of mass velocity maintains a constant mean value during the simulation. For example, let's consider the picture of the swarm configuration after 6000 time steps in the two cases $l_c = 10$ and $l_c = 1000$. We can notice a strong difference in the two situations. In the first one the net collective motion is still recognizable, but the behaviour of the swarm is not coherent as in the other picture. Moreover, if we look at the left pictures in Figures (3.15) and (3.16), at that time the x-velocity component in the first graph is about equal to the half of the analogous value in the second case. The final picture even shows a sharper gap. In the $l_c = 10$ the swarm already stopped, and the particles are wandering around the center of mass. Instead, in the $l_c = 1000$ case the swarm continues to move in the positive x-direction with almost the same initial velocity value.

3.3 Numerical simulations of statistical results

In this last section I want to report numerical outputs that verify analytical results from the center of mass velocity statistical analysis we carried out in chapter 2. For each of the three parameters regimes I performed three different simulations, in order to test the influence of the total number of swarm particles N . As statistical quantities we considered the expected value and the variance of the center of mass

velocity. In the previous section I already showed how setting $N = 1000$ guarantees that the microscopic dynamics is well approximated by the deterministic center of mass equation. It is reasonable since such a number of system components is sufficient to leads the noise average near zero. Now I analysed results setting N respectively equal to 500, 100 and 10, to check if analytical equations well predict the system behaviour also in case of a smaller swarm. All the simulations have been performed setting $dt = 0.01$ and averaging results of 10^5 realizations of the *Ornstein–Uhlenbeck process* described by the center of mass velocity equation (2.13). For each realization, the initial velocity value is a normally distributed random variable .

3.3.1 The accelerated regime

Here I present results about the $\alpha > \beta$ case that, how we have already seen in the previous section, determines an exponential acceleration of the swarm. I set $\alpha = 1$ and $\beta = 0.5$ as above. For the center of mass velocity expected value we consider the equation

$$\mathbb{E}[V] = \mathbb{E}[V_0]e^{\frac{(\alpha-\beta)}{m}t}, \quad (3.3)$$

while for the variance we have

$$\text{Var}(V) = \left[\text{Var}(V_0) + \frac{1}{2mN(\alpha - \beta)} \left(1 - e^{-\frac{2(\alpha-\beta)}{m}t} \right) \right] e^{\frac{2(\alpha-\beta)}{m}t}. \quad (3.4)$$

In Figure (3.19) results about variance and expected value of the swarm center of mass velocity from numerical simulations and analytical functions are compared.

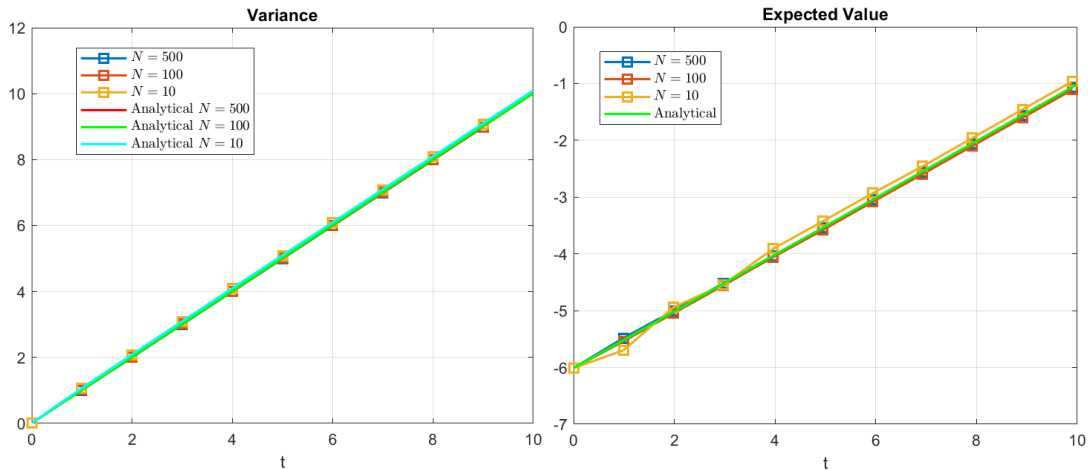


Figure 3.19: Variance and expected value of the swarm center of mass velocity from numerical simulations and analytical results. Semi-log plots.

The variance expression (3.4) depends on the number of particles N , and so each of the three analytical trends have been compared with the corresponding numerical case. We can notice that all the numerical outputs well match the analytical results, exhibiting an exponential growth. Analogous conclusions can be formed also for the velocity expected value, even if its analytical expression doesn't depends on N , as showed in equation (3.3).

3.3.2 The wandering center of mass regime

In this second case I set $\alpha = 0.5$ and $\beta = 1$, in order to simulate the damped regime. We can again consider the two previous equations as velocity variance and expected value analytical functions. Again numerical simulation outputs are

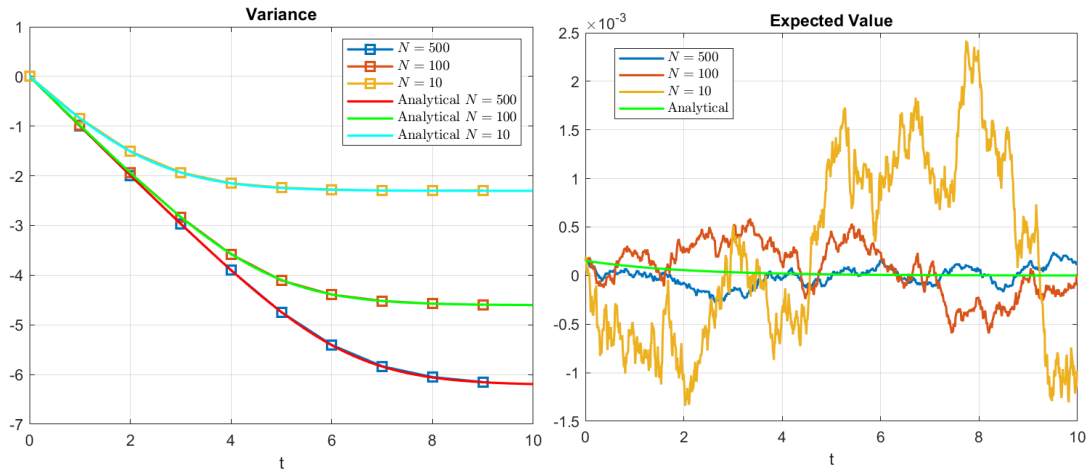


Figure 3.20: Velocity variance (semi-log plot) and expected value of the swarm center of mass. Comparison between analytical and numerical results.

in good agreement with analytical results (just notice that the expected value is scaled by a 10^{-3} factor). However, in this case the variance rapidly decrease to the constant value ($\text{Var}(V_0) - 1/2mN(\beta - \alpha)$) that depends on initial conditions and model parameters. The right picture shows the velocity expected value trend over time. Analytical function exhibits an exponential decay towards $\mathbb{E}[V_0]$, that is a near-zero value since it is extracted from a standard normal distribution and averaged on all the simulations. We can notice that numerical outputs oscillate around such a mean value, and fluctuations are stronger for a smaller value of N . This is because the noise term is scaled with the squared root of the number of particles, as reported in equation (2.13). Consequently a smaller amount of particles determines an higher noise influence on the swarm center of mass dynamics.

3.3.3 The invariant regime

Finally I report variance and expected value results for the case $\alpha = \beta = 1$. The expected value equation (3.3) reduces to

$$\mathbb{E}[V] = \mathbb{E}[V_0], \quad (3.5)$$

and so it describes a constant trend for the mean swarm center of mass velocity. For what concerns the variance, we can't use equation (3.4), since the difference $(\alpha - \beta)$ appears as denominator. Consequently we have to consider equation (2.27):

$$\text{Var}(V) = \text{Var}(V_0) + \frac{1}{m^2 N} t, \quad (3.6)$$

which predicts a linear growth for the velocity variance. We can observe in the right picture of Figure (3.21) that this trend is well fitted by numerical outputs, in each of the three cases with different N values. Right picture represents velocity

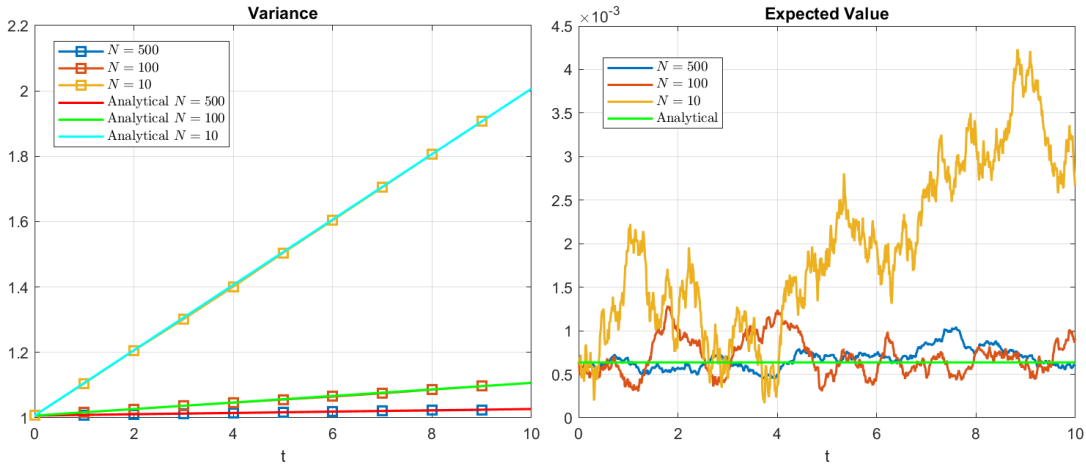


Figure 3.21: Velocity variance and expected value of the swarm center of mass in case of invariant regime.

expected value of the center of mass velocity. The analytical function has constant value, as derived, and numerical results again perform small amplitude fluctuations around the mean initial value. We can notice that the $N = 500$ case better fit the analytical trend, since the noise term is averaged on a greater number of particles. In conclusion, after this comparison between analytical and numerical results, we can state that the derived variance and expected value functions of the center of mass velocity well approximate the collective dynamics (described via *Langevin-type* equation (2.13)) even in the case of $N < 1000$.

Chapter 4

Conclusions and perspectives

In this paper I presented some results from my investigation period at BCAM (Basque Center for Applied Mathematics). In the second chapter I reported the new mathematical model we derived, which describes the collective dynamics of a swarm of self-propelled particles. We adopted a microscopic point of view, and consequently our model consists in a *Langevin-type* equation. We have chosen the mathematical terms which appear in it from the available literature on the topic (see for instance, [3], [8]), adapting them to our modelling assumptions. In particular in the dynamical equation there is a friction term, that accounts for the viscous damping force, a potential term, described as a potential gradient and that models repulsive/attractive social forces inside the swarm, and an alignment contribution, which is of fundamental importance in giving rise to collective dynamics. In fact, the alignment term couples the microscopic dynamics of the single particles, and it results in the emergence of self-organization and coherent behaviour of the entire swarm. We have chosen to model it as a weighted average of the neighbours velocity. Finally, our model comprehend a stochastic noise, which we defined as a *Wiener process*. It is also a crucial term, since in broad terms it introduces some randomness in the individual dynamics. For example, it could model the capability of the single particle to not perfectly obey to the social swarm stimuli, or, since we are considering active particles, their characteristic of not being completely prone to inertial effects. Then, summing the Langevin equations of all the particles, we obtained the stochastic differential equation describing the dynamics of the swarm center of mass. It predicts an exponential trend over time whose exponent depends on the difference between α and β , respectively the alignment and friction coefficients. This has allowed us to identify three different dynamical regimes depending on the balance between these two model parameters. The first one,

in which the alignment contribution overcomes the friction effect, describes an exponential acceleration of the swarm. It takes place once the swarm spontaneously align and start to move in a random direction depending on initial conditions. The second one, the $\alpha < \beta$ regime, predicts that the mean swarm velocity progressively approaches the zero value, as a results of the damping effect. Finally, the third one is characterized by a balance, on average, between the alignment term and the friction force. In this regime the dynamics of the center of mass remains constant over time and it depends on initial conditions. In the final part of the chapter I reported mathematical results we obtain performing a statistical analysis of the swarm center of mass dynamics. In particular we derived the expected value and the variance of the center of mass position and velocity over time. Since we adopted an underdamped modelling approach, this allowed us to focus on the stochastic noise role, and we found pretty interesting results. We observed that since a real swarm has to be finite, in the sense that it can count only a limited number of particles, the stochastic fluctuations increase the uncertainty of position and velocity of the swarm center of mass. We also noticed that a numerous ensemble tends to be less affected by the noise effect, since the corresponding term is inversely proportional to the total number of particles. Moreover, we found that in the $\alpha < \beta$ regime, the dynamics equation for the center of mass is formally equivalent to the one describing an *Ornstein–Uhlenbeck process*. In fact, also in this case, for long times, the variance of the center of mass position depends linearly on time and so the stochastic process becomes statistically indistinguishable from a *Brownian motion*. In the third chapter I reported results about numerical simulations, in order to compare them with analytical predictions. Numerical outputs have shown to be in good agreement. I also analysed the response of the model on the basis of a relaxation of the modelling assumptions. More specifically, I tested the current model in case of two different alignment characteristic lengths, observing how the difference in numerical output depends on the given dynamical regime. Finally I compared simulations outputs and analytical results about the statistical analysis numerically solving the swarm center of mass equation (2.13) in case of different number of particles. We observed that the analytical equations describing the velocity expected value and variance well approximate the swarm dynamics. To conclude, I want to introduce a couple of feasible future developments of the present work:

- The first one concerns a different implementation of the stochastic noise. In fact, instead of modeling it as an additive noise it can be introduced as a perturbation of the alignment function argument. So, we get

$$\mathfrak{f}_i^A(\mathbf{x}, \mathbf{v}) \longrightarrow \mathfrak{f}_i^A(\mathbf{x}, \mathbf{v} + \varepsilon(\mathbf{x})\boldsymbol{\eta}_i) = \sum_{i \neq j}^{N-1} (\mathbf{v}_j + \varepsilon(\mathbf{x})\boldsymbol{\eta}_j) e^{-\frac{|\mathbf{x}|}{l_c}}, \quad (4.1)$$

where the stochastic noise models the uncertainty in the perception of neighbours velocities. In an analogous way the noise term can also be thought to affect the position of other particles.

- The second one consists in developing a kinetic model for the collective swarm dynamics. When we consider really large swarm, for example in the case of cell populations, numerically solving the dynamical equations for each particle can be quite cumbersome. Then, it is possible to change modelling scale, from a microscopic point of view, to a mesoscopic one. In this way, we can derive a *Boltzmann-type* equation which involves the microscopic particle dynamics. Using an evolution equation for the probability density function of the form (1.2), it is possible to compute macroscopic quantities, such as the mean velocity of the swarm as a function of space and time.

I think collective motions are a really fascinating topic, both for their ubiquitous in nature and for their beauty. I'm also really interested in how simple interaction rules between particles can determine the emergence of coherent behaviour and ordered patterns. I think the understanding of collective motion of self-propelled particles is really important, both as a theoretical explanation of natural phenomena, which is of great significance, and as a useful tool directly applicable in several fields. For example, it can help in the developing of artificial swarm, in the spirit of biomimicry (see [10]). Moreover, these kind of models can reproduce various structures and behaviours observed in cell populations ([1]), and it can also point out the relative importance of different factors in determining a given collective dynamics.

Appendix A

Stochastic Noise

In order to contextualize the noise term of equation (2.1), I want to report one meaningful example, in which it has a central role (see [23]). As I previously pointed out, the microscopic description involves a stochastic differential equation describing individual trajectories, since position and velocity of the single particle are stochastic processes because of the presence of the noise term. In 1906 Paul Langevin proposed his own mathematical description of Brownian motion, that has been firstly observed by the Scottish botanist Robert Brown in 1827, while he was studying pollen grains suspended in water. The corresponding SDE involves a friction or viscous term, proportional to the particle velocity, and a stochastic fluctuation term, which models the effect of collisions with the medium parcels (very numerous and smaller than the "pollen grain"). Here I consider one dimensional equations without loss of generality, since results can be easily extended to higher dimensions. So, the governing equations are:

$$\begin{cases} dx = v dt \\ m dv = -\beta v dt + \sigma dW(t), \end{cases} \quad (\text{A.1})$$

where,

$$W(t) = \int_0^t \xi(s) ds. \quad (\text{A.2})$$

I wrote the *Langevin equation* in differential form, since the Brownian motion is nowhere differentiable with probability 1. The term $\xi(t)$ is a Gaussian white noise with zero mean, so that $\langle \xi(t) \rangle = 0$ and $\langle \xi(t)\xi(t') \rangle = \delta(t - t')$, while σ is the noise strength, that accounts for the intensity of the fluctuations (here we have an *additive noise*, since the factor multiplying the increment $dW(t)$ is a constant). Moreover, m is the particle mass, and β is the friction coefficient. This stochastic process is also referred as *Ornstein-Uhlenbeck process*, since these two authors provided a statistical analysis of it.

Usually these equations are applied in the *overdamped* limit regime (when $m \rightarrow 0$), and so, they reduce to

$$dx = \frac{\sigma}{\beta} dW(t) = \sqrt{2D} dW(t), \quad (\text{A.3})$$

considering $D = \frac{\sigma^2}{2\beta^2}$. This microscopic equation gives rise to the well known diffusion equation

$$\frac{\partial \rho}{\partial t} = D \frac{\partial^2 \rho}{\partial x^2}, \quad (\text{A.4})$$

which is its macroscopic analogous. Integrating equation (A.3), we obtain:

$$x(t) = x_0 + \sqrt{2D}W(t), \quad (\text{A.5})$$

where $W(t)$ is a *Wiener process*. It's interesting to notice that the well known Brownian motion, on a microscopic scale, takes place when the position is mathematically expressed as a Wiener process.

Now we can compute mean quantities related to different realizations of the noise term, so we have:

$$\mathbb{E}[x] = \mathbb{E}[x_0 + \sqrt{2D}W(t)] = \mathbb{E}[x_0] \quad (\text{A.6})$$

$$\text{Var}(x) = \mathbb{E}[(x - \mathbb{E}[x])^2] = \mathbb{E}[x^2] - \mathbb{E}[x]^2 = 2D\mathbb{E}[W^2] = 2Dt. \quad (\text{A.7})$$

Then, considering this type of stochastic processes, we observe that the expected value is equal to the initial expected value, while the variance grows linearly over time. Coming back to the equations describing the *Ornstein-Uhlenbeck process* (A.1) we can again compute these two statistical quantities. Integrating the second equation, we have

$$v(t) = v_0 e^{-\frac{\beta}{m}t} + \sigma W(t), \quad (\text{A.8})$$

and so,

$$\mathbb{E}[v] = \mathbb{E}[v_0] e^{-\frac{\beta}{m}t}, \quad (\text{A.9})$$

since the expected value of a Wiener process is equal to zero. In this expression m/β is the *persistence time*, which describes how long the correlation between velocities remains appreciable in the Ornstein-Uhlenbeck process. Indeed, for example, $\mathbb{E}[vv_0]/v_0^2 = e^{-\frac{\beta}{m}t}$ is a normalized measure of correlation between velocity v and its initial value.

Now we can proceed with the calculation of the expected value of the position, after have inserted the velocity expression (A.8) in the first equation of (A.1), and it gives us

$$\mathbb{E}[x] = \mathbb{E}[x_0] + \int_0^t \mathbb{E}[v] dt = \mathbb{E}[x_0] + \frac{m}{\beta} (1 - e^{-\frac{\beta}{m}t}) \mathbb{E}[v_0]. \quad (\text{A.10})$$

Now we have all the ingredients to compute also the variance of the position. I don't report here all the calculations, but I want to highlight its behaviour over time. For small times ($t \ll m/\beta$) we observe

$$\text{Var}(x) \sim t^2, \quad (\text{A.11})$$

and we can recognize a super-diffusive regime; this comes from the fact that during initial moments particles cover a distance proportional to time, indeed:

$$\mathbb{E}[x] - \mathbb{E}[x_0] = \mathbb{E}[(x - x_0)] = \frac{m}{\beta} \left(1 - e^{-\frac{\beta}{m}t}\right) \mathbb{E}[v_0] \approx \mathbb{E}[v_0]t. \quad (\text{A.12})$$

In the last equality we expanded the left term via the linear Taylor expansion $e^x \approx 1 + x$, for $t \rightarrow 0$. Instead, in the long time limit ($t \gg m/\beta$) the dependence on time becomes linear (standard diffusion). This result shows how, at very large times, the *Ornstein-Uhlenbeck process* is statistically equivalent to a *random walk*, and it's not possible to distinguish if the particle moved with a certain velocity or if it jumped randomly around. We can also notice that, unlike the previous case (A.3), in which the friction term was not considered, now we obtained an expected value of the position dependent on time, even if the decay is exponential.

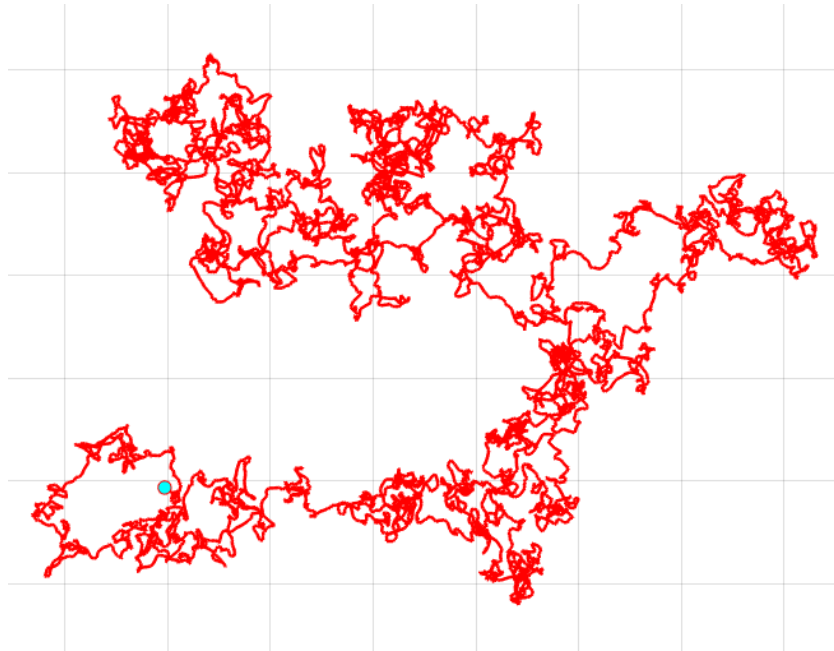


Figure A.1: Trajectory of a single particle which dynamics is described by a 2D *Ornstein-Uhlenbeck* process. Images obtained after 10^4 time steps, $\beta = 0.5$, $m = 1$, $\sigma = 1$. The final position of the particle is represented with the light blue circle.

Appendix B

Numerical simulation of stochastic processes

In this section I want to briefly present the numerical analysis theory I applied in order to solve the stochastic equations that govern the dynamics of the single particle and of the center of mass of the swarm. In the following I will refer to the article [4], which offers a clear overview of the topic.

We modeled the stochastic fluctuation as a *standard Wiener process*, that is a stochastic process $\mathbf{W}(t) \in \mathbb{R}^d$, with $d \in \mathbb{N}$, continuously dependent on time. In our case $d = 2$, but hereafter I will consider the one-dimensional case, without loss generality, since it can be thought as the k -th scalar component of a noise vector. The *Wiener process* $W(t)$ has the following properties:

- $W(0) = 0$, so it is equal to zero at the initial moment;
- $dW_t = W(t + dt) - W(t) \sim \sqrt{dt}\mathcal{N}(0,1)$, so it is a random variable normally distributed with zero mean and variance equal to dt ;
- two different increments dW_t and dW_s are independent, since they are different realizations of independent random variables.

Obviously, in our case we consider discrete random variables, and the sum of all the increments gives place to a *discretized Brownian path*, as represented in Figure (B.1). The trajectory is defined as the cumulative sum of increments at any time step, and here it is plotted in a 2D domain. This process is statistically equivalent to a *Ornstein–Uhlenbeck process* for long times, but it is described by an equation of the type (A.3).

In order to obtain a solution for the system (A.1), we have to solve a stochastic differential equation of this shape

$$dX(t) = f(X(t))dt + g(X(t))dW(t), \quad X(0) = X_0, \quad (\text{B.1})$$

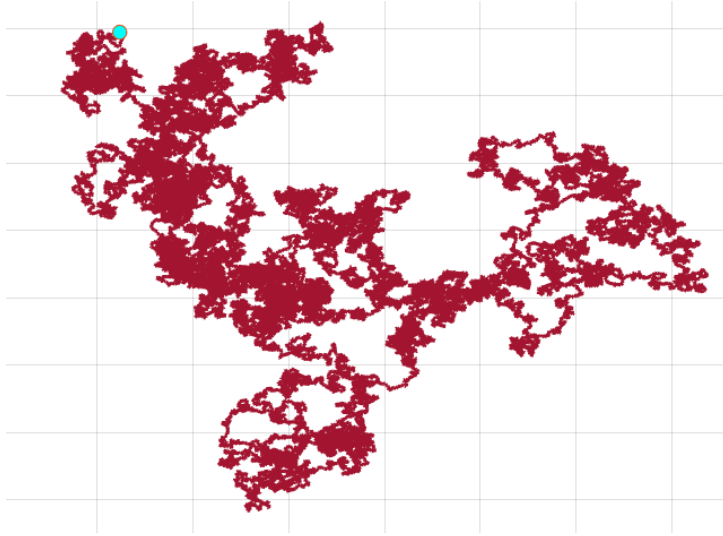


Figure B.1: Discretized Brownian path after $5 \cdot 10^4$ iterations. The final position is represented with the cyan dot.

where $X(t)$ is a stochastic process (in our case it represents the velocity of the i -th particle), with initial condition X_0 . Writing equation (B.1) in integral form, we obtain

$$X(t) = X_0 + \int_0^t f(X(s))ds + \int_0^t g(X(s))dW(s) \quad (\text{B.2})$$

In our model the coefficient $g(X(t))$ that multiplies the increment $dW(t)$ doesn't depend on the stochastic process, and so, having an *additive noise*, we get that the *Itô* and the *Stratonovich* interpretations of the stochastic integrals in (B.2) coincide. I want to emphasize that if $g = 0$ and the initial condition X_0 is not a random variable, we recover a ordinary differential equation describing a deterministic problem.

For the numerical solution I adopted the *Euler-Maruyama method*, that is an extension of *Euler method* to stochastic differential equations. The considered numerical method so takes the form

$$X_i = X_{i-1} + f(X_{i-1})\Delta t + g(W_i - W_{i-1}), \quad i = 1, 2, \dots, N_{\text{steps}}, \quad (\text{B.3})$$

and we can observe that it is the discretized version of

$$X(i) = X(i-1) + \int_t^{t+\Delta t} f(X(s))ds + \int_t^{t+\Delta t} g dW(s). \quad (\text{B.4})$$

For convenience, we always chose the time step size Δt for the numerical method to be equal to the increment dt for the Brownian path, but it is not strictly necessary, since one can consider also an integer multiple of it (this guarantees that the two sets of points coincide).

Bibliography

- [1] Tamás Vicsek, András Czirók, Eshel Ben-Jacob, Inon Cohen, and Ofer Shochet. «Novel Type of Phase Transition in a System of Self-Driven Particles». en. In: *Physical Review Letters* 75.6 (Aug. 1995), pp. 1226–1229 (cit. on pp. iii, 6, 49).
- [2] András Czirók and Tamás Vicsek. «Collective behavior of interacting self-propelled particles». en. In: *Physica A: Statistical Mechanics and its Applications* 281.1-4 (June 2000), pp. 17–29 (cit. on p. 8).
- [3] Herbert Levine, Wouter-Jan Rappel, and Inon Cohen. «Self-organization in systems of self-propelled particles». en. In: *Physical Review E* 63.1 (Dec. 2000), p. 017101 (cit. on pp. 12, 14, 47).
- [4] Desmond J. Higham. «An Algorithmic Introduction to Numerical Simulation of Stochastic Differential Equations». en. In: *SIAM Review* 43.3 (Jan. 2001), pp. 525–546 (cit. on p. 53).
- [5] Scott Camazine, ed. *Self-organization in biological systems*. eng. 2. print., and 1. paperback print. Princeton studies in complexity. Princeton, NJ: Princeton Univ. Press, 2003 (cit. on p. 2).
- [6] Mark Freidlin. «Some Remarks on the Smoluchowski-Kramers Approximation». en. In: *Journal of Statistical Physics* 117.3-4 (Nov. 2004), pp. 617–634 (cit. on p. 21).
- [7] Iain D. Couzin, Jens Krause, Nigel R. Franks, and Simon A. Levin. «Effective leadership and decision-making in animal groups on the move». en. In: *Nature* 433.7025 (Feb. 2005), pp. 513–516 (cit. on p. 10).
- [8] Udo Erdmann, Werner Ebeling, and Alexander S. Mikhailov. «Noise-induced transition from translational to rotational motion of swarms». en. In: *Physical Review E* 71.5 (May 2005), p. 051904 (cit. on pp. 12, 15, 47).
- [9] Chad M. Topaz, Andrea L. Bertozzi, and Mark A. Lewis. «A nonlocal continuum model for biological aggregation». In: (2005). Publisher: arXiv Version Number: 1 (cit. on pp. 3, 5).

- [10] M. R. D’Orsogna, Y. L. Chuang, A. L. Bertozzi, and L. S. Chayes. «Self-Propelled Particles with Soft-Core Interactions: Patterns, Stability, and Collapse». en. In: *Physical Review Letters* 96.10 (Mar. 2006), p. 104302 (cit. on pp. 7, 12, 14, 49).
- [11] B. Szabó, G. J. Szöllösi, B. Gönci, Zs. Jurányi, D. Selmeczi, and Tamás Vicsek. «Phase transition in the collective migration of tissue cells: Experiment and model». en. In: *Physical Review E* 74.6 (Dec. 2006), p. 061908 (cit. on p. 3).
- [12] Felipe Cucker and Steve Smale. «Emergent Behavior in Flocks». In: *IEEE Transactions on Automatic Control* 52.5 (May 2007), pp. 852–862 (cit. on p. 8).
- [13] Felipe Cucker and Steve Smale. «On the mathematics of emergence». en. In: *Japanese Journal of Mathematics* 2.1 (Mar. 2007), pp. 197–227 (cit. on p. iii).
- [14] M. Ballerini et al. «Interaction ruling animal collective behavior depends on topological rather than metric distance: Evidence from a field study». en. In: *Proceedings of the National Academy of Sciences* 105.4 (Jan. 2008), pp. 1232–1237 (cit. on pp. 3, 15).
- [15] Irene Giardina. «Collective behavior in animal groups: Theoretical models and empirical studies». en. In: *HFSP Journal* 2.4 (Aug. 2008), pp. 205–219 (cit. on p. 3).
- [16] José A. Carrillo, M. R. D’Orsogna, V. Panferov, ,ICREA-Departament de Matemàtiques, Universitat Autònoma de Barcelona, E-08193 Bellaterra, and ,Department of Mathematics, California State University, Northridge, CA 91330-8313. «Double milling in self-propelled swarms from kinetic theory». en. In: *Kinetic & Related Models* 2.2 (2009), pp. 363–378 (cit. on p. 5).
- [17] Giovanni Naldi, Lorenzo Pareschi, and Giuseppe Toscani. *Mathematical modeling of collective behavior in socio-economic and life sciences*. eng. Modeling and simulation in science, engineering and technology. Boston: Birkhäuser, 2010 (cit. on pp. 3, 5, 8, 14).
- [18] Marzena Ciszak, Diego Comparini, Barbara Mazzolai, Frantisek Baluska, F. Tito Arecchi, Tamás Vicsek, and Stefano Mancuso. «Swarming Behavior in Plant Roots». en. In: *PLoS ONE* 7.1 (Jan. 2012). Ed. by Eshel Ben-Jacob, e29759 (cit. on p. 3).
- [19] R. C. Fetecau and A. Guo. «A Mathematical Model for Flight Guidance in Honeybee Swarms». en. In: *Bulletin of Mathematical Biology* (Aug. 2012) (cit. on p. 10).
- [20] Tamás Vicsek and Anna Zafeiris. «Collective motion». en. In: *Physics Reports* 517.3-4 (Aug. 2012), pp. 71–140 (cit. on p. 3).

- [21] Bernt K. Øksendal. *Stochastic differential equations: an introduction with applications*. eng. 6. ed., 6. corr. print. Universitext. Berlin Heidelberg: Springer, 2013 (cit. on p. 19).
- [22] Előd Méhes and Tamás Vicsek. «Collective motion of cells: from experiments to models». en. In: *Integr. Biol.* 6.9 (2014), pp. 831–854 (cit. on pp. 2, 10).
- [23] Vicenç Méndez, Daniel Campos, and Frederic Bartumeus. *Stochastic Foundations in Movement Ecology: Anomalous Diffusion, Front Propagation and Random Searches*. en. Springer Series in Synergetics. Berlin, Heidelberg: Springer Berlin Heidelberg, 2014 (cit. on pp. 3, 50).
- [24] Alexandria Volkening and Björn Sandstede. «Modelling stripe formation in zebrafish: an agent-based approach». en. In: *Journal of The Royal Society Interface* 12.112 (Nov. 2015), p. 20150812 (cit. on p. 2).
- [25] Dapeng Bi, Xingbo Yang, M. Cristina Marchetti, and M. Lisa Manning. «Motility-Driven Glass and Jamming Transitions in Biological Tissues». en. In: *Physical Review X* 6.2 (Apr. 2016), p. 021011 (cit. on p. 3).
- [26] Damian Stichel, Alistair M. Middleton, Benedikt F. Müller, Sofia Depner, Ursula Klingmüller, Kai Breuhahn, and Franziska Matthäus. «An individual-based model for collective cancer cell migration explains speed dynamics and phenotype variability in response to growth factors». en. In: *npj Systems Biology and Applications* 3.1 (Mar. 2017), p. 5 (cit. on p. 3).
- [27] Sara Bernardi, Annachiara Colombi, and Marco Scianna. «A discrete particle model reproducing collective dynamics of a bee swarm». en. In: *Computers in Biology and Medicine* 93 (Feb. 2018), pp. 158–174 (cit. on p. 3).
- [28] Sara Bernardi, Annachiara Colombi, and Marco Scianna. «A particle model analysing the behavioural rules underlying the collective flight of a bee swarm towards the new nest». en. In: *Journal of Biological Dynamics* 12.1 (Jan. 2018), pp. 632–662 (cit. on pp. 3, 10).
- [29] David Karig, K. Michael Martini, Ting Lu, Nicholas A. DeLateur, Nigel Goldenfeld, and Ron Weiss. «Stochastic Turing patterns in a synthetic bacterial population». en. In: *Proceedings of the National Academy of Sciences* 115.26 (June 2018), pp. 6572–6577 (cit. on p. 2).
- [30] Sara Bernardi and Marco Scianna. «An agent-based approach for modelling collective dynamics in animal groups distinguishing individual speed and orientation». en. In: *Philosophical Transactions of the Royal Society B: Biological Sciences* 375.1807 (Sept. 2020), p. 20190383 (cit. on p. 3).
- [31] A. Colombi, M. Scianna, K. J. Painter, and L. Preziosi. «Modelling chase-and-run migration in heterogeneous populations». en. In: *Journal of Mathematical Biology* 80.1-2 (Jan. 2020), pp. 423–456 (cit. on p. 3).